Global characterization of the cyclic-di-GMP regulome by bi-directionally evolving a social trait in *Pseudomonas fluorescens*

Collin Kessler[1], Wook Kim[1*]

[1] Department of Biological Sciences, Duquesne University, 600 Forbes Ave., Pittsburgh, PA 15282, USA

*** Correspondence:**

kimw1@duq.edu

Abstract

Microbial communities comprise densely packed cells where competition for space and resources are fierce. These communities, generally referred to as biofilms, provide advantages to individual cells against immunological and antimicrobial intervention, dehydration, and predation. High intracellular pools of cyclic diguanylate monophosphate (c-di-GMP) cause individual cells to aggregate during biofilm formation through the production of diverse extracellular polymers. Genes that encode c-di-GMP enzymes or their regulators are commonly mutated during chronic infections due to enhanced resistance to phagocytosis and antibiotics. Genome annotations predict the presence of numerous c-di-GMP catalytic enzymes in most bacterial species, but the functionality and regulatory control of the vast majority remain unconfirmed. Here, we begin to fill this gap by utilizing an experimental evolution system in *Pseudomonas fluorescens* Pf0-1, which repeatedly produces a unique social trait through bidirectional transitions between two distinct phenotypes converging on c-di-GMP modulation. Parallel evolution of 33 lineages captured 147 unique mutations among 191 evolved isolates in genes that are empirically demonstrated, bioinformatically predicted, or previously unknown to impact the intracellular pool of c-di-GMP. Quantitative chemistry confirmed that each mutation causing the phenotypic shift

either amplifies or reduces c-di-GMP production. We integrate our data with current models of known regulatory and catalytic systems, describe a previously unknown relationship between branched-chain amino acids and c-di-GMP production, and predict functions of several new proteins that either regulate or catalyze c-di-GMP production. Sequential mutations that continuously disrupt or recover c-di-GMP production across discrete functional elements suggest a complex and underappreciated interconnectivity within the c-di-GMP regulome.

Introduction

Microbes that persist in chronic infections utilize diverse signaling mechanisms to adapt and respond to a dynamic environment. Opportunistic pathogens that evade host immune responses can persist for long periods of time (Monack et al., 2004) and chronic infections typically require continuous antibiotic therapy to suppress symptoms (Grant & Hung, 2013). Investigating bacterial phenotypes and adaptations associated with persistent infections is essential for developing alternative therapeutic strategies to counter the rise in antibiotic resistance. Individuals with cystic fibrosis (CF) typically develop persistent and detrimental bacterial infections (Edwards et al., 2017; J. Malone, 2015; Starkey et al., 2009). Clinical isolates of *Pseudomonas aeruginosa* from CF patients characteristically display enhanced resistance to phagocytosis and antibiotics frequently due to mutations in cyclic di-guanosine monophosphate (c-di-GMP) associated genes (Gloag et al., 2019; Römling et al., 2013). Recent machine learning models have demonstrated that physicians could utilize c-di-GMP related mutation data to adjust treatments based on the predicted disease outcomes (Dahlstrom et al., 2018; Schumacher et al., 2021; Yan et al., 2017).

C-di-GMP is a ubiquitous secondary messenger in bacteria and multiple regulatory pathways converge on modulating intracellular c-di-GMP levels (Armbruster et al., 2019; Hall & Lee, 2018; Yan et al., 2017). High intracellular levels of c-di-GMP repress flagellar genes while stimulating the expression

49 of biofilm-formation genes (Irie et al., 2010; Kuchma et al., 2015; Merritt et al., 2007). Activating c-di-
50 GMP production during a lung infection enables microbes to adhere to the mucosal surface through
51 lipopolysaccharide (LPS) modifications and the production of type IV pili and adhesins (Borlee et al.,
52 2010; Hall & Lee, 2018; McCarthy et al., 2017; Skotnicka et al., 2016). Numerous c-di-GMP binding
53 proteins and riboswitches respond to intracellular levels of c-di-GMP to also regulate cellular
54 morphology, virulence factors, antibiotic production, and the cell cycle (Dahlstrom et al., 2016; Tamayo,
55 2019). Many taxa possess dozens of enzymes that are predicted to control its synthesis and metabolism.
56 C-di-GMP is catalyzed from two molecules of GTP by a diguanylate cyclase (DGC) and hydrolyzed by a
57 phosphodiesterase (PDE). DGCs and PDEs are identified by the GGDEF or EAL/HD-GYP domains,
58 respectively, and many microbes have genes that encode hybrid proteins with both DGC and PDE
59 functions.

60 Bioinformatics analyses reveal that *Pseudomonas* spp. typically possess greater than 50
61 predicted DGCs or PDEs, but mechanistic understanding of their regulation is limited to only few
62 examples (Sarenko et al., 2017). PDEs and DGCs like RmcA and GcbC, respectively, are under allosteric
63 control where c-di-GMP concentrations initiate or prevent further enzymatic activity (Chan et al., 2005;
64 Christen et al., 2006; Giacalone et al., 2018; Mantoni et al., 2018). Other DGCs and PDEs like DgcH, CfcR,
65 MorA, PleD, SadC, WspR, and YfiN are governed by specific signaling pathways and regulators (De et al.,
66 2008; Giardina et al., 2013; Huertas-Rosales et al., 2017; Kessler et al., 2021; Merritt et al., 2010;
67 Moscoso et al., 2014; Ravichandran et al., 2015; Wassmann et al., 2007). However, the vast majority of
68 bioinformatically predicted DGCs and PDEs have not been empirically validated and their regulatory
69 mechanisms remain unknown (Dahlstrom et al., 2018).

70 Here, we report the utilization of a bidirectional experimental evolution system in *Pseudomonas*
71 *fluorescens* Pf0-1 (Kim et al., 2016) to identify 147 unique mutations in genes that are empirically
72 demonstrated, bioinformatically predicted, or previously unknown to impact c-di-GMP levels. We

73 expand the current model of c-di-GMP production by the Wsp signaling system and demonstrate that
74 branched-chain amino acid (BCAA) production is a recurrent target of mutations that positively correlate
75 to measured c-di-GMP levels. We also describe several proteins with no previous associations to c-di-
76 GMP that likely act as internal regulators. Lastly, we predict the interconnectivity of the c-di-GMP
77 regulome through sequential mutations that disrupt or recover c-di-GMP regulation across functionally
78 discrete systems. This work demonstrates how a simple experimental evolution system can
79 systematically map out c-di-GMP regulatory and enzymatic elements and uncover remarkable molecular
80 innovations.
81
82 **Results and Discussion**
83 **Bidirectional evolution of mucoid and dry phenotypes occurs through intracellular c-di-GMP pool**
84 **oscillation**
85 A previous experimental evolution study described the bidirectional evolution of mucoid (M)
86 and dry (D) colony phenotypes in *P. fluorescens* Pf0-1, which likely occurs through c-di-GMP oscillation
87 (Kim et al., 2016) (Fig. 1A). An aging colony of M cells repeatedly produces spreading fans at the
88 perimeter, which comprise the original M cells along with new D mutant cells that produce a dry and
89 wrinkly colony morphology on their own. Additionally, an aging colony of D cells also repeatedly
90 generates spreading fans, which comprise the original D cells along with a new mutant that appears
91 phenotypically identical to the ancestral M. This bidirectional selection of M and D phenotypes occurs
92 continuously because M and D cells self-organize in space and physically work together to spread out
93 from the nutrient-poor and crowded conditions of dense colony growth, and neither type is capable of
94 spreading out on their own (Kim et al., 2016). In contrast, a colony of initially mixed M and D cells readily
95 spreads out in a radial pattern without requiring additional mutations (Fig. 1A). Genetic analyses of
96 several D isolates and a second-generation M isolate revealed characteristic mutations in *wsp* genes to

97 suggest that c-di-GMP production is likely elevated in D and reduced in M (Kim et al., 2016). With the
98 expectation that a large-scale utilization of this experimental evolution system could identify diverse
99 mechanisms of c-di-GMP modulation, we set up 25 parallelly evolving lineages of M.

100 As anticipated, we observed bidirectional transitions between M and D phenotypes across all
101 lineages. In total, we isolated over 600 strains, genome sequenced a subset of 191 strains, and
102 quantified c-di-GMP in a subset of 56 strains. Remarkably, we detected a single mutation associated
103 with each phenotypic transition, with the exception of only few silent mutations across all 191 genome
104 sequences (Fig. S1, Table S1, Table S1 – Source Data 1). Genome sequencing successive strains within
105 each lineage provided an internal control, which confirmed the exclusive presence of the respective
106 preceding mutations. 147 unique mutations were detected across diverse genes that have been
107 empirically demonstrated, bioinformatically predicted, or are previously unknown to impact c-di-GMP
108 levels, including unannotated hypothetical genes. Motility assays showed that all D strains were non-
109 motile and all M strains were motile, and LC-MS/MS quantification confirmed that c-di-GMP was
110 elevated in all D strains relative to their respective parent M strain (Table S1). For the sake of an
111 accessible narrative, we will primarily focus our description on five select lineages that have been
112 simplified (Fig. 1B). Corresponding c-di-GMP measurements are shown in Fig. 1C and colony
113 morphologies are shown in Fig. S2. Among the 35 strains represented here, we observed a significant
114 increase in c-di-GMP in the 21 D strains compared to the 14 M strains (Fig. 1C). There is a slight overlap
115 in c-di-GMP concentrations when comparing all M and D strains together, but c-di-GMP was elevated in
116 all D strains respective to their immediate parent M strain. This observation may reflect the importance
117 of subcellular localization of c-di-GMP (Massie et al., 2012) compared to the overall intracellular pool
118 (Yan et al., 2017) for certain physiological properties, and variations in the wrinkly colony morphology as
119 observed among our collection of D strains (Fig. S2).

120 The combination of our mutation data and corresponding c-di-GMP quantification data could
121 serve as a powerful resource for deducing protein and pathway functions. Furthermore, successive
122 patterns of mutations across generations of independently evolving lineages could reveal previously
123 unknown connectivity between discrete regulatory and catalytic systems. Notably, many of our
124 mutations that sequentially disrupt or recover c-di-GMP production target the Wsp signaling system, the
125 most extensively studied c-di-GMP regulator in *Pseudomonas* spp. (Kessler et al., 2021). We first focus
126 on multiple series of sequential mutations in the Wsp system to reveal remarkable evolutionary
127 innovations to modulate c-di-GMP production.

128 **Diverse mutations converge on the Wsp signal transduction system that dynamically rewire signal**
129 **flow to produce a spectrum of functional states**

130 Among the 35 mutations identified across our subset of five lineages (Fig. 1B), 24 fall within the
131 Wsp signal transduction system (Fig. 2). The Wsp system was first reported two decades ago (Spiers et
132 al., 2002) and continues to serve as the primary model system of c-di-GMP regulation in *Pseudomonas*
133 spp. (Kessler et al., 2021). The Wsp system comprises seven proteins encoded in a monocistronic operon
134 under the control of an unidentified transcriptional regulator (Bantinaki et al., 2007). The
135 transmembrane protein WspA has an extracellular sensory domain that detects surface contact and may
136 respond to other unidentified signals (Armbruster et al., 2019). Homology with the enteric chemotaxis
137 system predicts that once WspA is stimulated by surface contact, it undergoes a conformational change
138 that exposes cytosolic methylation helices that are necessary for signal transduction (Rice & Dahlquist,
139 1991). The methyl-transferase WspC is then predicted to dock at the 5' tail of WspA and methylate the
140 WspA trimer-of-dimers complex (Feng et al., 1999). The signal is then relayed through the coupling
141 proteins WspB and WspD, and subsequently to WspE, which functions as a histidine kinase (Alexander
142 et al., 2010). WspE phosphorylates the DGC WspR to stimulate c-di-GMP production (Malone et al.,
143 2007). Simultaneously, WspE phosphorylates the methyl-esterase WspF, which de-methylates WspA and

144 terminates the signaling cascade (Bantinaki et al., 2007). Significant work has been carried out to
145 characterize the biochemical functions of WspE and WspR in particular, and WspE is a common
146 mutational target in a clinical setting (Kessler et al., 2021). More recently, studies have begun to explore
147 the functional role of WspA during signal activation and subcellular localization, revealing that both
148 properties are dependent on WspB and WspD proteins (O'Connor et al., 2012; Armbruster et al., 2019).
149 These studies also suggest that WspB and WspD likely possess unique functions, but they remain
150 unresolved.

151 Given that a mutation in any one of the seven Wsp protein coding genes could potentially
152 increase or decrease c-di-GMP production through WspR (Fig. 2), we expected *wsp* genes to be a
153 common target in our parallel experimental evolution study. However, we were surprised to find that
154 the vast majority of the first transitions from the ancestral M to D occurred through a *wsp* mutation
155 (Table S1). Such a striking pattern suggests that the Wsp system has the greatest capacity to contribute
156 to the overall intracellular pool of c-di-GMP under our experimental conditions, and this is also reflected
157 in our quantification data where the highest c-di-GMP production is typically associated with *wsp*
158 mutations (Table S1). We thus set up an independent lineage to commence with an engineered *ΔwspC*
159 M strain (Fig. 3, strain 1.0), with the expectation that the deletion of *wspC* would prevent further
160 mutations within the Wsp system, since the removal of the methyltransferase should prevent WspA
161 signaling (Fig. 2). However, this was not the case. The first D progeny strain 1.1 harbors a missense
162 mutation in WspA (A381V) within its signaling domain, which is consistent with the results from a
163 previous study (O'Connor et al., 2012). Mutations in this domain structurally stimulate WspE, so the
164 A381V mutation likely locks WspA in a constitutively active conformation even in the absence of
165 methylation by WspC. The subsequent M progeny strain 1.2 harbors a missense mutation in WspB
166 (L136P), which likely disrupts the interaction between WspA and WspE to terminate c-di-GMP
167 production. We next observed an in-frame deletion of amino acid residues 647-696 spanning the

168 phosphoreceiver domain of WspE in the D progeny strain 1.3. The restoration of c-di-GMP production in
169 this strain suggests that the observed deletion likely forces WspE to conform an activated state.
170 Accordingly, mutations within the phosphoreceiver domain of CheY, a WspE homolog in *Escherichia coli*,
171 can activate the protein without phosphorylation (Bellsolell et al., 1994; Re et al., 2002). In addition, the
172 DGC activity of WspR in *P. aeruginosa* does not necessarily depend on phosphorylation (De et al., 2008;
173 Huangyutitham et al., 2013). The subsequent M progeny strain 1.4 carries a frameshift mutation in
174 *wspE*, which should terminally shut down the Wsp system, and the c-di-GMP level was reduced as
175 predicted. C-di-GMP production was restored in this lineage once again in the following D strain 1.5
176 through a missense mutation in DgcH (V459G), a bioinformatically predicted DGC in *P. aeruginosa* PAO1
177 that impacts biofilm formation (Wei et al., 2019). While DgcH shares a namesake with the DGCs DgcA,
178 DgcB, and DgcC, no known interactions exist between these proteins and DgcH. The V459G mutation
179 significantly increases enzymatic output either by directly activating DgcH or relieving an unidentified
180 repressor. Sequence analysis shows that DgcH also possesses an inhibitory I-site, indicating that it may
181 be under allosteric control of c-di-GMP as discussed below.
182 Lineages 2, 3, 4, and 5 were commenced with an unaltered ancestral M strain (Fig. 3). Mutations
183 in lineages 2 to 4 were primarily detected in Wsp proteins with strongly predictable functional
184 outcomes. The first D strain 2.1 of lineage 2 carries a mutation in *wspA* that appears to activate WspA
185 through an in-frame deletion of the methylation helices. This mutation likely affects the helical coiled-
186 coil domain of WspA to mimic a permanently methylated state (Kessler et al., 2021), resulting in
187 increased signal transduction and the overproduction of c-di-GMP. The following shift to the M
188 phenotype is associated with a missense mutation in WspD (W90L), which likely disrupts the relay of
189 signal from WspA to WspE. The D strain 2.3 restores c-di-GMP production through the missense
190 mutation in Pfl01_3147 (A383S), which is annotated as a hypothetical protein, but we found homology
191 to an N-ethylammeline chlorohydrolase. We will refer to this protein as NarA (N-ethylammeline

192 chlorohydrolase associated c-di-GMP regulator). The potential role of this novel c-di-GMP regulator is
193 explored in the last section.
194 Similar to strain 2.1, the first D strain 3.1 of lineage 3 carries a unique in-frame deletion of *wspA*
195 that partially spans the methylation sites of WspA, which results in increased c-di-GMP (Fig. 3). Strain 3.2
196 transitions to the M phenotype through a missense mutation in the signaling domain of WspA (L387R).
197 This mutation likely weakens or abolishes signal transduction to WspE. In the following D strain 3.3, the
198 missense mutation in WspE (G601V) occurs in the putative WspF/WspR docking site (Kessler et al.,
199 2021). This mutation likely allows WspF and WspR to interact with WspE more easily, thereby increasing
200 the phosphorylation of both proteins. Since the methylation sites of WspA were initially removed in the
201 ancestral D strain 2.1, activation of WspF would not shut down signal transduction while the activation
202 of WspR would result in the observed overproduction of c-di-GMP (Fig. 2).
203 The first D strain 4.1 of lineage 4 carries an in-frame deletion mutation in *dgcH* that removes
204 amino acid residues 524-537 of DgcH (Fig. 3). Interestingly, the GGDEF diguanylate cyclase domain of
205 DgcH spans residues 537-693. The observed in-frame deletion adjacent to this domain appears to
206 activate c-di-GMP production, though we cannot currently speculate on the mechanisms due to limited
207 understanding of DgcH. We observed a reduction in c-di-GMP in the following M strain 4.2, which has a
208 missense mutation in DgcH (L634P). A search against NCBI's conserved domain database identifies that
209 the residues 619-643 contain the inhibitory I-site, with residue N637 as the predicted interaction site.
210 Our mutation data supports this annotation and the likelihood that DgcH is under allosteric control by c-
211 di-GMP. The L634P mutation may mimic a c-di-GMP bound state, causing the observed reduction in c-di-
212 GMP. We cannot discount the possibility of additional regulatory mechanisms since we observe
213 numerous other missense and in-frame deletion mutations across the length of DgcH (Table S1). The
214 following D strain 4.3 restores c-di-GMP production through a missense mutation in WspA (V380A),
215 which affects the signaling domain to activate WspA like the A381V mutation observed in the D strain

216 1.1. C-di-GMP is reduced again in the M strain 4.4, which carries a missense mutation in the HATPase
217 domain of WspE (D390N), likely disrupting the capability to cleave the phosphate from ATP. Despite
218 potentially disabling WspE's kinase activity, the D strain 4.5 recovers c-di-GMP production through an in-
219 frame deletion of the methylation helix of WspA. The observed increase in c-di-GMP is minimal, which is
220 consistent in a *wspE* knock down strain. WspE is then further disabled by another missense mutation
221 V441A in the M strain 4.6, which again affects the HATPase domain to decrease c-di-GMP production.
222 Incredibly, the following D strain 4.7 recovers c-di-GMP production through the missense mutation
223 S472C in the HATPase domain of WspE by replacing the polar amino acid serine with the non-polar
224 amino acid cysteine. Non-polar amino acids are important in protein-ATP binding and this mutation may
225 allow for WspE to interact with ATP more efficiently in the presence of the other acquired mutations
226 (Chauhan et al., 2009).

227 **Mutations in non-*wsp* genes with known or unknown associations with c-di-GMP production integrate**
228 **with *wsp* mutations to modulate c-di-GMP levels**

229 Sequential patterns of mutations and c-di-GMP quantification across our 33 lineages indicate
230 that the DGCs WspR, DgcH, and MorA represent the most dominant contributors to the intracellular c-
231 di-GMP pool (Table S1). Other known or predicted DGCs are typically targeted to modulate c-di-GMP
232 levels after the Wsp system and DgcH become genetically dysfunctional. We also observed mutations in
233 bioinformatically annotated genes with no known associations to c-di-GMP modulation. These patterns
234 are best represented in lineage 5, the longest sequenced lineage in this study with 13 linear phenotypic
235 transitions (Fig. 3, Table S1). Like other lineages, mutations initially accumulate within *wsp* genes to
236 deregulate the Wsp system, then other known or predicted DGCs SadC, DgcH, YfiN, GcbC, and MorA are
237 genetically modified to both reduce or stimulate c-di-GMP production. The first transition to the D strain
238 5.1 occurs through a missense mutation in WspF (P105S), which disrupts its methyl-esterase activity to
239 keep WspA in an activated state (Fig. 2). This activation is undone in the follow M strain 5.2 by an in-

240 frame deletion of 3 nucleotides in *wspA* that removes the amino acid residue S329 of WspA, which falls
241 in the linker region between the methylation sites and the signaling domain (Kessler et al., 2021). This
242 mutation likely interrupts the methylated signal received from WspC and prevents or weakens the
243 transmission of signal to WspE. C-di-GMP production is restored in the subsequent D strain 5.3 through
244 the partial deletion of the WspA methylation sites. This mutation likely produces a conformational
245 change in WspA that permits the relay of the signal past the previously acquired S329 deletion in the
246 helical coiled-coil domain. The next M strain 5.4 carries an in-frame deletion which removes seven
247 amino acids in WspD. While the functional importance of this region in WspD remains unresolved, its
248 impact on Wsp signaling is clear as reflected by the reduction in c-di-GMP. This region is likely important
249 for the signal transmission between WspA and WspE, either by destabilizing the tertiary structure of
250 WspD or by removing a docking domain required for interactions with WspA and/or WspE. Subsequent
251 strains D 5.5 and M 5.6 carry mutations that activate then deactivate the DGC SadC, respectively. The
252 activating mutation occurs in the 5'UTR of *sadC* and likely increases the expression of the DGC as
253 evidenced by increased intracellular c-di-GMP (Fig. 3). This activation is then undone through an in-
254 frame deletion of the L25 residue in SadC. Surprisingly, strain 5.7 returns this lineage to the D phenotype
255 through a missense mutation in IlvH (G150S), which is predicted to function in the biosynthesis of
256 branched chain amino acids (BCAA). We observed three independent missense mutations in IlvH across
257 our study that exclusively cause a phenotypic shift from M to D and reduced motility (Table S1).
258 Accordingly, quantification of c-di-GMP shows that each of these three mutations significantly increases
259 c-di-GMP respective to their immediate M parent (Fig. 4). These results indicate that a previously
260 unknown relationship between BCAA biosynthesis and c-di-GMP production may exist. We explore this
261 relationship in greater detail below.
262 Lineage 5 returns to the M phenotype in strain 5.8 through a missense mutation in the
263 hypothetical protein Pfl01_0730 (D115N) (Fig. 3). This protein, hereon ParA (PAP2 associated c-di-GMP

264 regulator), shares homology with the PAP2 superfamily of proteins, suggesting that it may be involved in
265 phospholipid turnover and may impact the bioavailability of phosphate within the cell (Carman & Han,
266 2006). Although we found the relative decrease in c-di-GMP in strain 5.8 to be not statistically significant
267 from its parent likely due to technical noise (Fig. 4), the observed mutation clearly drives the phenotypic
268 transition from D to M. Furthermore, if this mutation does not impact c-di-GMP levels, then we would
269 not expect a further transition through elevated c-di-GMP production. In fact, we captured two
270 independent transitions back to the D phenotype, both with significantly increased c-di-GMP levels (Fig.
271 3). Strains 5.9a and 5.9b are sister strains that have developed unique chimeric Wsp proteins that likely
272 restore Wsp signaling. Both chimeric proteins (WspA::D and WspB::D) contain identical partial segments
273 of WspD commencing at residue 158, situated immediately adjacent to the in-frame deletion detected
274 in their common ancestral strain 5.4 that previously deactivated the Wsp system (Fig. 3). To determine
275 whether or not these chimeric proteins alone are sufficient to drive the phenotypic shift from M to D,
276 we replaced the corresponding native Wsp proteins in the ancestral M strain with each chimeric protein.
277 In parallel, we also replaced the corresponding naturally modified Wsp proteins in the immediate
278 parental M strain 5.8 with each chimeric protein. Both engineered strains in the ancestral M background
279 retained the M phenotype, but both engineered strains in the M strain 5.8 background recapitulated the
280 D transition that was observed in strains 5.9a and 5.9b (Table 1). These results indicate that the two
281 chimeric Wsp proteins require additional mutation(s) observed within this lineage to produce c-di-GMP.
282 Both the WspA::D and WspB::D chimeras have lost WspC, which is not surprising since the methylation
283 sites of WspA were removed previously in D strain 5.3. Similarly, WspB is completely removed in the
284 WspA::D chimera and nearly 75% of WspB has been removed in the WspB::D chimera. At this stage, it
285 remains unclear whether or not the observed mutations in *ilvH* and/or *parA* are required for the
286 function of the two Wsp chimeras. However, we present additional evidence below that strengthens the
287 potential relationship between IlvH and the Wsp system.

288 The WspB::D chimera strain 5.9b was next used to evolve the M progeny strains. Sister strains
289 5.10a and 5.10b were isolated and each were found to carry frameshift deletions in *ilvI* that decreased c-
290 di-GMP levels (Fig. 4). The two *ilvI* mutants carry a deletion of 17 or 23 nucleotides that start at the same
291 position, which should abolish IlvI's function. IlvI and IlvH form a complex that catalyzes the first step of
292 BCAA biosynthesis, where IlvH serves as the regulatory subunit and IlvI serves as the catalytic subunit
293 (Ricca et al., 1988). IlvH in *E. coli* has been bioinformatically predicted to respond to c-di-GMP levels due
294 to the presence of the inhibitory I-site that could manifest allosteric regulation (Fang et al., 2014). We
295 identified that IlvH of *P. fluorescens* Pf01 also contains the I-site RXXD motif at residues 103-106. None
296 of the independently identified IlvH mutations (A36E, S149R, and G150S) in our study fall within this
297 motif, but all three mutations significantly increase c-di-GMP levels (Fig. 4). Beyond the potential
298 allosteric regulation of IlvH by c-di-GMP, there is no known relationship between BCAA biosynthesis and
299 c-di-GMP production to the best of our knowledge. However, we suspected that the IlvH mutations,
300 including the G150S mutation observed earlier in this lineage, increase BCAA production to stimulate c-
301 di-GMP production through an unknown mechanism, since we subsequently observe frameshift
302 mutations in the catalytic subunit (IlvI) that returns this lineage back to the M phenotype with reduced
303 c-di-GMP levels.
304 The frameshift mutations in *ilvI* should lead to BCAA auxotrophy, which is likely masked by the
305 nutrient-rich medium utilized in our experimental evolution system. To test this prediction, we grew
306 strains 5.10a and 5.10b in a chemically defined minimal medium without BCAA. We did not observe any
307 growth unless BCAA was exogenously supplemented (Fig. S3), confirming that our *ilvI* mutants are
308 unable to synthesize BCAA. We next tested if exogenous supplementation of BCAA alone could restore
309 c-di-GMP production in the *ilvI* mutant (M strain 5.10a). Since the *ilvI* mutant cannot grow in the
310 minimal medium without BCAA supplementation, we also included our prototype M and D ancestors
311 (Fig. 1A), as relative controls in addition to the *ilvH* mutant (D strain 5.7) and *parA* mutant (M strain 5.8)

312 from the same lineage. Exogenous supplementation of BCAA in the *ilvI* mutant indeed restored c-di-
313 GMP production at comparable levels to both D and the *ilvH* mutant (D strain 5.7) (Fig. 5). In contrast, c-
314 di-GMP levels remained the same in both M and the *parA* mutant (M strain 5.8) regardless of BCAA
315 supplementation (Fig. 5). These results show that overabundance of BCAA does not correlate with c-di-
316 GMP production and defeats our initial prediction that the missense mutations in *ilvH* increase BCAA
317 production to stimulate c-di-GMP production. Although BCAA supplementation restores c-di-GMP
318 production in the *ilvI* mutant strain in a minimal medium, the reduction of c-di-GMP levels observed in
319 the same *ilvI* mutant under our nutrient-rich experimental evolution conditions (Fig. 4) is not likely
320 associated with losing the ability to synthesize BCAA. Accordingly, reconstructing the two frameshift *ilvI*
321 mutations independently in the ancestral D strain does not cause a shift to the M phenotype, but the
322 initially observed shift to the M phenotype is recapitulated when these mutations are introduced into
323 their direct parental D strains (Table 1). Since IlvI forms a complex with IlvH, the observed frameshift
324 mutations in *ilvI* likely decouples the complex, and consequently impacts IlvH's potential function to
325 modulate c-di-GMP production. Lineage five returns to the D phenotype following the *ilvI* mutations
326 through mutations in *wspE* or *dcgH* (Fig. 3). As observed in other lineages, we commonly isolate *wspE*
327 mutants when the upstream signaling of Wsp is disrupted. Here, we capture the mutations M123I,
328 D289N, and Δ524-537AA in WspE. These mutations fall in the HPT domain, the dimerization domain, and
329 the REC domain, respectively, and likely activate WspE in the absence or reduction of upstream Wsp
330 signal (Kessler et al., 2021). The fourth observed mutation that returns lineage five to the D phenotype is
331 an in-frame deletion of *dgcH* that is identical to the deletion reported in the D strain 4.1. These four
332 independent transition steps into the D phenotype clearly indicate that the catalytic activity of IlvI is not
333 required for c-di-GMP production.

334 We also set up another lineage to commence with an engineered *ΔwspCD* M strain (Table S1,
335 strain 27.0), with the same initial expectation as lineage 1 that the deletion of both *wspC* and *wspD*

336 would prevent further mutations within the Wsp system (Fig. 2). In contrast to the *ΔwspC* M strain
337 lineage 1, the first shift to the D phenotype is associated with a non-*wsp* mutation. We observed a
338 missense mutation in DgcH (Q454P), and the following shift to the M phenotype occurred through
339 another missense mutation in DgcH (Q148P), which showed the expected reduction in c-di-GMP
340 production. In addition to the four unique missense mutations in DgcH described thus far, we observed
341 several other missense mutations that cause phenotypic shifts in both directions, and unique in-frame
342 deletions that cause a shift to the D phenotype across many other lineages (Table S1). These
343 observations collectively indicate that DgcH is another main contributor to the total c-di-GMP pool. We
344 observed a very interesting pattern in the next two sequential steps, with the first shift to the D
345 phenotype occurring through a missense mutation in IlvH (A36E), which restores c-di-GMP production
346 (Fig. 4), and the following shift back to the M phenotype being associated with a mutation which
347 converts the stop codon of *wspB* with a cysteine residue to extend its open reading frame, but out of
348 frame with *wspE* (both *wspC* and *wspD* are already deleted). A common trend exists between lineages 5
349 (Fig. 3) and 27 (Table S1) in that multiple mutations first occur in Wsp proteins, which is proceeded by
350 mutations in a non-Wsp DGC (SadC or DgcH, respectively), then unique missense mutations occur in IlvH
351 to stimulate c-di-GMP production. Reconstructing the three IlvH missense mutations in the ancestral M
352 strain does not lead to a shift to the D phenotype, but reconstructing these mutations in their direct
353 parental M strain recapitulates the initially observed shift to the D phenotype (Table 1). The common
354 targets of mutations between the two lineages that converge on IlvH mutations are Wsp proteins, which
355 implies that the c-di-GMP stimulating mutations in IlvH associate with a de-regulated Wsp system.
356 Furthermore, the undoing of the IlvH (A36E)-induced c-di-GMP production by the stop codon mutation
357 in *wspB* implies potential IlvH-Wsp interactions that are unlikely to be metabolic in nature.

358 **A macro assessment of sequential mutation patterns across all 33 parallel lineages captures potential**
359 **associations within the c-di-GMP regulome**

360 A long standing question in the field is why microbes possess so many independent DGC and/or
361 PDE machineries. A systematic mutational analysis of genes that were bioinformatically predicted to be
362 DGCs in *P. fluorescens* demonstrated that most have little impact on the intracellular c-di-GMP pool
363 (Newell et al., 2011), and a significant number of DGCs/PDEs in *E. coli* are present in an inactive form
364 (Hengge et al., 2016). In addition, independent DGCs could regulate a sub-cellularly localized role
365 (Massie et al., 2012) that could also contribute to the total intracellular pool to regulate diverse
366 physiological pathways across a gradient (Yan et al., 2017). Our study indicates that many known or
367 predicted DGCs could be independently stimulated to regulate a common phenotypic shift, which
368 appears to operate across a broad range of c-di-GMP levels (Fig. 1C). We also capture mutations in
369 genes with no previously known c-di-GMP associations that significantly impact the c-di-GMP pool, and
370 these genes are affected repeatedly across multiple lineages (Table S1), which strongly suggests that
371 they are indeed components of the c-di-GMP regulome. To visualize patterns of sequential mutations
372 and potential associations within the c-di-GMP regulome, we compiled all sequential orders of the
373 mutation events across the 33 parallel lineages into a single node-edge plot (Fig. 6A). This type of plot
374 can be used to consolidate decision trees used to train a random forest machine learning model (Casarin
375 et al., 2021). Although much more extensive data are required to generate a such model, the depicted
376 relationships are predictive of sequential mutations that could, for example, be observed in clinical
377 isolates that typically accumulate numerous mutations throughout a chronic infection (Malone, 2015).
378 The nodes in Fig. 6A represent the mutated genes in our experiment. The edges (i.e. lines) of the
379 plot report if the mutation causes an M (blue) or D (orange) phenotype, and the thickness of the edge
380 reflects the frequency of the observed pattern (Table S2). Proteins that are integrated into this plot –
381 meaning that many edges connect to a specific node – collectively form the main ring. Nodes associated
382 with a single edge fall out of this ring, and mutations in these proteins typically occur at the end of a
383 lineage or a branched sub-lineage that was not sequenced. Since we did not isolate any progeny strains

384 from these ten mutants that fall outside the main ring, we do not further evaluate their potential role in
385 c-di-GMP modulation. Notably, the largest nodes in this plot constitute Wsp proteins, DgcH, and other
386 known diguanylate cyclase's like YfiN, GcbC, MorA, and SadC. We observe that mutations in WspA that
387 increase c-di-GMP are primarily followed by mutations in WspB, WspD, or WspE that result in the M
388 phenotype (blue edge) with decreased c-di-GMP. Mutations in WspF that fail to return the Wsp system
389 back to the ground state are followed by mutations in WspC to abolish WspA's activity, mutations in
390 WspA to force an off conformation, or mutations in WspR to physically shut down c-di-GMP production.
391 The frequency of these patterns correlates well with the direction of signal flow in the Wsp system (Fig.
392 2), where the primary mutations constitutively activate the Wsp system and subsequent mutations
393 disrupt the signal relay among the downstream components. Then, activating mutations occur in WspE
394 that decouple WspE from the upstream components to restore c-di-GMP production, which is followed
395 by mutations in WspE that deactivate it or mutations in WspR to shut down c-di-GMP production. The
396 majority of DGCs like SadC and YfiN have blue recursive edges that cause an M phenotype, which
397 indicates that mutations occur in the same protein to shut down its activity, immediately following a
398 mutation that initially stimulated its activity. The high frequency of blue recursive edges associated each
399 DGC and yellow edges between distinct DGCs collectively indicate that each DGC simply replaces
400 another to restore c-di-GMP production. Blue edges between DGCs are extremely rare, which suggests
401 that individual DGCs do not directly interact with another. Notably, there are several proteins with both
402 yellow and blue edges that are integrated in this plot and have not been shown to have a role in c-di-
403 GMP regulation or production. We next infer potential function of these proteins with respect to c-di-
404 GMP modulation.

405 ***NarA*** (N-ethylammeline chlorohydrolase associated c-di-GMP regulator)

406 In strain 2.3, we observe that the A383S mutation in NarA increases c-di-GMP levels (Fig. 6B),
407 which confirms that this hypothetical protein is indeed biologically active. This NarA mutation follows

408 the M-shifted W90L mutation in WspD, which suggests that NarA is either able to restore Wsp signaling
409 or activate other DGCs to increase c-di-GMP levels. We have no reason to suspect that NarA directly
410 catalyzes c-di-GMP since it lacks any c-di-GMP associated domains or motifs. The progeny of this NarA
411 mutant carries a nonsense mutation in *wspD*, reverting this strain back to an M phenotype (Table S1).
412 Thus, the A383S mutation in NarA associates specifically with *wspD* mutations to both restore and shut
413 down c-di-GMP production. NarA is predicted to catalyze N-ethylammeline, a derivative of ammeline,
414 and a recent study theorized that ammeline is likely an essential building block required for the
415 synthesis of cyclic complexes (Petelski & Fonseca Guerra, 2019). Although the metabolic connections are
416 unknown, there is a strong indication that NarA interacts with WspD at some capacity to modulate c-di-
417 GMP levels.
418 ***CdrB*** (Two-partner secretion system transporter)
419 Pfl01_0652 in *P. fluorescens* encodes a protein that is homologous to the transporter protein
420 CdrB in *P. aeruginosa* (PA4624). In *P. aeruginosa*, CdrA and CdrB are encoded in a single operon and
421 form a two-partner secretion (TPS) system associated with biofilm formation (Reichhardt et al., 2018).
422 CdrA (c-di-GMP regulated TPS A) is an extracellular adhesin known to respond to modifications made by
423 the periplasmic protease LapG which is activated by the transmembrane c-di-GMP receptor LapD
424 (Cooley et al., 2016). It has been reported that high intracellular levels of c-di-GMP enable CdrA to bind
425 and crosslink secreted Psl, thereby increasing cell-cell adhesion (Reichhardt et al., 2018). *cdrA/B*
426 expression also increases proportionally with intracellular levels of c-di-GMP during biofilm formation
427 (Borlee et al., 2010). CdrB is a transporter with domains that indicate it is a type V secretion system
428 transporter. CdrB is likely involved in the transport of the adhesin CdrA but has no identified role in c-di-
429 GMP modulation. In our lineage 6, the missense mutation YfiN G157C increases c-di-GMP production,
430 which is immediately followed by the CdrB A290T missense mutation to decrease c-di-GMP levels (Fig.
431 6B). This suggests that an unaltered CdrB or its native transport activity is necessary for YfiN's DGC

432 activity. As reported in Table S1, mutations that follow the CdrB mutation occur in *morA* or *dgcH*, each
433 increasing c-di-GMP as indicated by the D-phenotype (Table S1). Therefore, the negative impact of our
434 CdrB mutation on YfiN could be recovered through the genetic activation of other DGCs, which may also
435 reflect interactions with CdrB.

436 ***DgcX* and *DgcY*** (Bioinformatically predicted DGCs)

437 Pfl01_3550 and Pfl01_3508 are both bioinformatically predicted to encode DGCs, but their
438 enzymatic function has not yet been demonstrated. Here, we establish that they are both functionally
439 active in c-di-GMP catalysis and annotate them as *dgcX* and *dgcY*, respectively, since proteins DgcA
440 through DgcW already exist. Pfl01_3550, hereon *dgcX*, is a commonly mutated gene in our dataset
441 which increases c-di-GMP (Table S1). We observe a blue recursive loop in the node-edge plot for DgcX,
442 which is consistent with other known DGCs (Fig. 6A). We isolated two independently evolved D mutants
443 with the same M350I mutation, and an M mutant with an in-frame deletion of L289. Phenotypic and
444 motility data support that the observed mutations in *dgcX* influence the intracellular c-di-GMP pool. The
445 genomic location of *dgcY* is in a region of hypothetical genes that appear to form an operon.
446 Interestingly, our *dgcY* mutant strains carry large deletions that span the 9 hypothetical genes within
447 this genomic region. The deletion of Pfl01_3505, Pfl01_3506, and the 5' UTR region of *dgcY* results in a
448 significant increase in c-di-GMP (Strain 6.5a, Fig. 6B). This likely removes the repression of *dgcY*
449 transcription by replacing the promoter region of *dgcY* with that of Pfl01_3505. C-di-GMP is significantly
450 decreased in the progeny strain 6.6a (Fig. 6B) after the deletion of Pfl01_3500, Pfl01_3501, Pfl01_3502,
451 Pfl01_3503, Pfl01_3504, Pfl01_3505, Pfl01_3506, Pfl01_3508, Pfl01_3509, and Pfl01_3510, which
452 includes *dgcY*. It is unclear whether or not the encoded proteins of hypothetical genes that flank *dgcY*
453 are functionally related to DgcY. We had initially suspected that these hypothetical genes could encode
454 a complex signal transduction system like Wsp, but we did not detect any homologous Wsp domains or
455 other c-di-GMP associated motifs.

456 ***CalM*** (c-di-GMP associated LysM)

457 The hypothetical gene Pfl01_1895, hereon *calM* (c-di-GMP associated LysM) is a commonly
458 mutated gene in our study (Table S1). The encoded protein contains domains with homology to the
459 LysM peptidoglycan-binding superfamily and contains a FimV C-terminal transmembrane domain that is
460 implicated in modulating motility (Buendia et al., 2018; Wehbi et al., 2011). The LysM proteins are
461 identified by the lysin motif which is associated with cell lysis. The presence of the LysM and FimV
462 domains suggests that this protein may respond to changes in peptidoglycan stress, which is essential
463 for maintaining cell shape and integrity. C-di-GMP is a well-known regulator of cellular morphology in
464 *Vibrio cholera* and *Caulobacter crescentus* (Conner et al., 2017; Wassmann et al., 2007). We observe a
465 duplication of five nucleotides within *calM* that results in a significant decrease in c-di-GMP (Fig. 6B).
466 Two repetitive clusters of CAGCG shifts to three clusters to cause a frameshift. This mutation follows a
467 *dcgH* in-frame deletion that dramatically increases c-di-GMP production, indicating that CalM is
468 necessary for DgcH's activity. Remarkably, three independently evolved progeny strains in this lineage
469 carry mutations that remove the initial five nucleotide insertion, returning each strain back to the D
470 phenotype likely by restoring DgcH's activity (Table S1).

471 ***RndA*** (RND transporter)

472 Pfl01_2749 is bioinformatically predicted to encode an RND transporter. RND transporters
473 function as efflux pumps to remove toxins, antibiotics, quorum sensing (QS) molecules, and other
474 metabolites (Soto, 2013). We observe that the nonsense mutation Q51* in Pfl01_2749, hereon *rndA*,
475 significantly decreases c-di-GMP levels (strain 11.2, Fig. 6B). A recent study speculates that QS molecules
476 contribute to a feedback loop to inhibit c-di-GMP production (Liang et al., 2020). Thus, an active RndA
477 could potentially modulate this feedback loop by expelling certain effector compounds to stimulate c-di-
478 GMP production. The *rndA* mutant shifts to the D phenotype through an in-frame deletion that removes

479 amino acid residues 524-537 in DgcH. This specific mutation was observed in multiple lineages to
480 exclusively stimulate c-di-GMP production.
481 To confirm whether the observed mutations in these atypical c-di-GMP associated genes alone
482 could modulate c-di-GMP levels, we reconstructed representative mutations in their respective
483 ancestral backgrounds. None of the engineered strains produced a phenotypic shift (Table 1), indicating
484 that additional mutation(s) within their respective lineage are required to impact c-di-GMP levels.
485 Accordingly, reconstructing the same mutations in their direct parental strains recapitulates the initially
486 observed phenotypic shifts (Table 1). Although additional research is required to prescribe specific
487 mechanisms, diverse cellular processes appear to be integrated with numerous catalytic machineries to
488 modulate the c-di-GMP pool.
489
490 **Conclusion**
491 C-di-GMP associated mutations are commonly observed in chronic infections (Gloag et al., 2019;
492 Römling et al., 2013), indicating that deregulating c-di-GMP production is a clinically significant genetic
493 adaptation. Although we have extensive knowledge on how specific enzymes make or break c-di-GMP
494 and how this molecule interacts with a large number of regulatory elements to modulate diverse
495 physiological processes, relatively little is known about how C-di-GMP production itself is regulated. This
496 study utilizes a repeatedly evolving social trait in *P. fluorescens* to identify 147 unique mutations that
497 modulate the intracellular c-di-GMP pool. We demonstrate how numerous proteins could
498 independently and collectively produce remarkable sequences of genetic innovation to oscillate c-di-
499 GMP levels.
500 Our extensive library of *wsp* mutations allows us to reinforce the current functional model of
501 the Wsp system, which particularly lacks resolution in WspA, WspB, and WspD (Kessler et al., 2021).
502 Although methylation of WspA remains to be empirically demonstrated, the WspA methylation helices

503 clearly have a functional role in Wsp signaling as they were commonly mutated to activate c-di-GMP
504 production. Based on our mutation data and homologies to Tsr-methylation in the chemotaxis system of
505 *E. coli* (Rice & Dahlquist, 1991), we predict that the following residues are methylated in WspA: CH_3-A:
506 Q285, E292, E299 and CH_3-B: Q502, E512. The linker region of WspA that connects the HAMP and
507 signaling domains contains the first set of E and Q residues, which undergo methyl esterification in Tsr
508 during chemotaxis. A second linker region between the signaling domain and predicted WspC-WspF
509 docking site contains the second set of E and Q residues. The addition of a bulky methyl group to the Tsr
510 methylation site of the coiled-coil alters the topology of the alpha helix which is relayed through the
511 linker domain and into the signaling domain (Levit & Stock, 2002). WspA is expected to undergo a similar
512 conformational change upon methylation and our data suggest that the deletion of the putative
513 methylation sites mimics a methylated state, which is relayed through its linker domain and into the
514 signaling domain that interacts with WspB, WspD, and WspE. The functional roles of WspB and WspD in
515 signal relay are largely modeled after homology to CheW of *E. coli*, which is the least characterized
516 protein in the chemotaxis system. A previous study explored the interaction sites between CheW, CheA
517 (WspE homolog), and Tsr through mutagenic screens (Liu & Parkinson, 1991). Mutations in CheW that
518 successfully disrupted signal transduction were largely limited to five unique amino acid clusters that
519 situate on the protein surface and are essential for the docking of CheW to Tsr (Li et al., 2007). WspB
520 and WspD also possess six and seven highly conserved amino acid clusters, respectively (Kessler et al.,
521 2021). We have identified WspB L135P and WspD W90L mutations that fall within these conserved
522 clusters that likely situate on the surface of WspB and WspD and natively act as docking sites for WspA
523 and WspE to permit signal relay. Consistent with our hypothesis, both mutations reduce c-di-GMP levels.
524 We also observed several other mutations in WspB and WspD that independently impact c-di-GMP
525 production. Our data confirm that both WspB and WspD are necessary for Wsp signal transduction.

526 Beyond the Wsp system, we have identified unique missense mutations and in-frame deletions
527 in multiple DGCs that fall outside their conserved catalytic domain. The sites of these mutations likely
528 represent regulatory domains that are critical for modulating enzymatic activity. Notably, DgcH is a
529 relatively understudied DGC, which greatly influenced the intracellular c-di-GMP pool in our system. The
530 L634P mutation occurring adjacent to the predicted I-site likely mimics a c-di-GMP bound state, thus
531 preventing catalytic activity as observed by reduction in c-di-GMP levels. The repeatedly observed in-
532 frame deletion of amino acids 524-537 exclusively increased c-di-GMP levels, which may act to override
533 the inhibition through the I-site or represents a unique domain for interaction with another repressive
534 element. We have also confirmed that several bioinformatically predicted DGCs to be indeed
535 enzymatically active. In particular, DgcY is encoded within a nine gene cluster of unknown function.
536 Although we could not identify any specific homologies, the large deletions we observed in this cluster
537 lead us to speculate that they encode a unique system that functions to regulate DgcY's activity.
538 Lastly, we have uncovered a set of unexpected or hypothetical proteins that clearly have the
539 capacity to influence c-di-GMP turnover. Three missense mutations in *ilvH* were identified to
540 independently stimulate c-di-GMP production, which appears to be independent of IlvH's primary role in
541 BCAA biosynthesis, but rather operates through an unknown interaction with the Wsp system. We have
542 identified the same I-site in IlvH as in DgcH, which suggests that IlvH physically interacts with c-di-GMP.
543 Similarly, CalM, CdrB, and RndA homologs in other organisms have been implicated to respond to c-di-
544 GMP levels, but they have never been associated with c-di-GMP modulation. We have confirmed that
545 the mutations observed in these proteins alone do not impact c-di-GMP levels, but do so in the presence
546 of other mutations. In particular, a DgcH-driven c-di-GMP production is negated by a frameshift
547 mutation in *calM*, which implies a potential interaction between these two proteins. Similarly, a YfiN-
548 driven c-di-GMP production is negated by a missense mutation in *cdrB*, and c-di-GMP production
549 appears to be restored again through a mutation in either *morA* or *dgcH*. Furthermore, a *narA* missense

550 mutation is flanked in sequence by independent mutations in *wspD* to modulate c-di-GMP production in
551 both directions.

552 An emerging concept here is that the intracellular pool of c-di-GMP, whether it be subcellularly
553 localized or in sum, appears to be modulated through the catalytic activities of many independent DGCs
554 that are in tune with diverse proteins. Such intricacies are masked by the activities of DGCs with high
555 output, but they could readily manifest otherwise. Although direct functional studies are necessary to
556 resolve the underlying mechanisms, this study reveals a complex and underappreciated
557 interconnectivity within the c-di-GMP regulome. Harvesting natural selection in the laboratory could
558 provide a unique path for discovering and disentangling complex molecular processes that are relevant
559 in a clinical setting.

560

561 **Material and Methods**

562 **Strains and culture conditions**

563 All *Pseudomonas fluorescens* Pf0-1 (Compeau et al., 1988) derivatives associated with parallel
564 experimental evolution are described in Table S1 and engineered strains are described in Table 1. Strains
565 were routinely grown in Lennox LB (Fisher BioReagents), *Pseudomonas* Minimal Medium (PMM) (Kirner
566 et al., 1996), or on *Pseudomonas* Agar F (PAF) (Difco). *Pseudomonas* F (PF) broth (a non-agar variant of
567 PAF) was prepared with the following: pancreatic digest of casein 10 g/L (Remel), proteose peptone No.
568 3 10 g/L (Remel), dipotassium phosphate 1.5 g/L (Sigma-Aldrich), and magnesium sulfate 1.5 g/L (Sigma-
569 Aldrich). Cultures were incubated at 30°C and shaken at 250 rpm when applicable.

570 **Parallel experimental evolution**

571 Pure cultures of the ancestral M strain or engineered M strains were grown overnight in 5mL LB
572 broth and 25uL volumes were spotted on PAF plates, then incubated at room temperature for 3 to 8
573 days to allow spreading fans to emerge. To ensure consistency across experiments, PAF plates were

574 always prepared and left to dry at room temperature for 2 days before being inoculated. One fan was
575 randomly sampled from each colony and streaked out on LB plates in duplicate. Sampling a fan always
576 produced two strains with either a mucoid (M) or dry (D) colony phenotype. A single isolated colony
577 exhibiting the D phenotype was randomly selected to start a new liquid culture and also frozen down.
578 This process was repeated to sample six independent fans (i.e. six lineages). Three of the six
579 independently isolated D strains were randomly selected and cultured as above to start the next round
580 of experimental evolution. We repeated the same sampling process as above except that new M
581 phenotypes were isolated instead. We bidirectionally selected M and D phenotypes for as many as 13
582 rounds for a single lineage, but the number of sampled fans at each step was reduced over time in a
583 varying manner across independent lineages. In total, approximately 600 independently evolved isolates
584 were frozen down across 33 parallel lineages. Every isolate was subjected to a motility assay in an LB
585 plate with 0.25% agar, and the prototype M and D ancestors were used as controls (Kim et al., 2016). In
586 addition, 25uL of pure cultures of each isolate, the ancestral strain with the opposite phenotype, and a
587 1:1 mixture of both were spotted onto PAF plates in triplicate and assessed for cooperative radial
588 spreading (Fig. 1A) to filter out hyper-motile and non-cooperative mutants (Kim et al., 2016). Colony
589 diameters were measured and recorded after four days of incubation at room temperature and
590 considered cooperative if the measured diameter of the 1:1 colony exceeded both the diameters of the
591 isolated mutant strain and the respective ancestral strain. Isolates that failed this test were removed
592 from this study.

593 **Reconstruction of naturally derived mutations in ancestral and direct parental backgrounds**

594 Experimentally evolved isolates were whole genome sequenced to identify the causal mutations as
595 described below. We reconstructed select naturally acquired mutations in the respective ancestral
596 background and also in the direct parental background using previously described methods (Kim et al.,
597 2016). PCR primers were developed from the sequence data to amplify mutations of interest and are

598 reported in Table S3. Isolates were grown overnight and underwent DNA extractions (Qiagen). Dream
599 Taq DNA Polymerase (ThermoFisher) was used in PCR reactions with purified DNA to generate insert
600 fragments carrying the mutations which ranged in size from 456bp to 934bp. PCR was carried out using
601 the recommended conditions of the Dream Taq amplification kit for amplicons below 2000bp. Inserts
602 were cloned into the pGEM-T Easy vector system (Promega) and then subcloned into the *Not*I site of the
603 suicide plasmid pSR47s (Matthews & Roy, 2000). Suicide plasmids were heat shocked into *E. coli*
604 S17.1λ*pir*, mated with the target strains reported in Table S3 on LB plates at 30°C for 16 hours, then
605 plated onto PMM plates supplemented with 50 ug/ml kanamycin. We observed that *ilvI* mutants could
606 not grow on PMM and therefore replaced the PMM selection plate with an LB plate supplemented with
607 50 ug/ml kanamycin and 100 ug/ml ampicillin for *ilvI* mutant constructs. Isolated colonies were grown
608 overnight, serially diluted and plated out on LB plates supplemented with 15% sucrose (w/v) for
609 counterselection. Isolated colonies were placed in cryo-storage as described above. Crude DNA extracts
610 were made for each strain where 100uL of overnight culture was boiled at 100°C, centrifuged at 15,000
611 RCF for 30 seconds, and 10uL of supernatant was used for PCR using the primers reported in Table S3.
612 PCR products underwent gel extraction and subsequent sanger sequencing (primers in Table S3) to
613 confirm that the mutation was successfully engineered into the target strain. Upon PCR confirmation,
614 pure cultures of cells from cryo-storage underwent DNA extraction (Qiagen) and were submitted for
615 WGS which confirmed that no additional mutations had accumulated in the target strains during mutant
616 construction.

617 **DNA extraction, whole genome sequencing, and variant calling**

618 Pure cultures were grown overnight in 5mL LB broth at 30°C. 1 mL was spun down to form a
619 pellet for DNA extraction. Pelleted cells were mechanically lysed with the Qiagen TissueLyser LT at 50
620 oscillations/second for 10 minutes. The Qiagen DNeasy UltraClean Microbial DNA extraction kit was
621 used following the standard operating procedures. Samples were then eluted into 30uL H_2O after a 5

622 minutes incubation at 4°C with the elution media and stored at -20°C prior to shipment. Genomic DNA
623 library preparations were carried out by the Microbial Genome Sequencing Center (Pittsburgh, PA)
624 following standard operating procedures. Pooled and indexed samples were sequenced on the NextSeq
625 2000 platform and demultiplexed prior to data delivery. The Trimmomatic algorithm was used to group
626 and quality filter paired reads at a Phred score of 20 using a 4bp sliding window. The BreSeq algorithm
627 was used to align the paired reads to the *P. fluorescens* Pf0-1 reference genome (CP000094.2) and
628 evaluate for single nucleotide polymorphisms (SNPs), insertions, deletions, or rearrangements. Output
629 sequence data from BreSeq is compiled as 'Table S1 – Source Data 1' and was manually evaluated for
630 each strain to determine the order of mutations for a given lineage.

631 **C-di-GMP extraction and LC-MS/MS**

632 An isolated colony of each strain was transferred to PF broth and grown overnight. Overnight
633 cultures were diluted to an OD_{600} of 0.04 in triplicate and incubated for 2-4 hours until the samples
634 reached an OD_{600} of 0.5, then promptly processed for c-di-GMP extraction. C-di-GMP extraction and
635 quantification procedures followed the protocols established by the Michigan State University Research
636 Technology Support Facility (MSU-RTSF): MSU_MSMC_009 protocol for di-nucleotide extractions and
637 MSU_MSMC_009a for LC-MS/MS, with the following modifications. All the steps of c-di-GMP extraction
638 were carried out at 4°C unless noted otherwise. 1mL of 0.5 OD_{600} culture was centrifuged at 15,000 RCF
639 for 30 seconds, and cell pellets were resuspended in 100uL of ice cold acetonitrile/methanol/water
640 (40:40:20 (v/v/v)) extraction buffer supplemented with a final concentration of 0.01% formic acid and
641 25nM c-di-GMP-Fluorinated internal standard (InvivoGen CAT: 1334145-18-4). Pelleted cells were
642 mechanically disturbed with the Qiagen TissueLyser LT at 50 oscillations/second for 2 minutes.
643 Resuspended slurries were incubated at -20°C for 20 minutes and pelleted at 15,000 RCF for 15 minutes
644 at 4°C. The supernatant was transferred to a pre-chilled tube then supplemented with 4uL of 15% w/v
645 ammonium bicarbonate (Sigma-Aldrich) buffer for stable cryo-storage. Extracts were stored at -80°C for

646 less than two weeks prior to LC-MS/MS analysis at MSU-RTSF. Sample degradation was observed with
647 repeated freeze-thaw cycles, so extracts were never thawed until LC-MS/MS analysis. All samples were
648 evaporated under vacuum (SpeedVac, no heat) and redissolved in 100uL mobile phase (10 mM TBA/15
649 mM acetic acid in water/methanol, 97:3 v/v, pH 5). LC-MS/MS quantification was carried out with the
650 Waters Xevo TQ-S instrument with the following settings: c-di-GMP-F at *m/z* transition of 693 to 346
651 with cone voltage of 108 and collision voltage of 33; c-di-GMP at *m/z* transition of 689 to 344 with cone
652 voltage of 83 and collision voltage of 31. C-di-GMP data was normalized to 25nM c-di-GMP-F by MSU-
653 RTSF to account for sample matrix effects and sample loss during preparation. OD_{600} measurements of
654 the initial samples were used to report the quantified c-di-GMP as nM/OD and visualized with GraphPad
655 Prism9.

656 **BCAA supplementation assay and c-di-GMP quantification**

657 Pure cultures were grown overnight in 5mL LB broth. 5uL of each culture was transferred into
658 5mL PMM. Cultures were supplemented with the BCAA valine, leucine, and isoleucine as previously
659 described (Kim & Levy, 2008). Assessment of growth during BCAA supplementation contained either
660 0uM (loading control), 180uM, 200uM, 220uM, 250uM, or 300uM in triplicate. Samples were incubated
661 at 30°C for 24 hours at 250 rpm shaking. Cultures were manually pipetted to resuspend cells and 300uL
662 of culture was transferred to a 96-well black wall clear bottom plate for OD_{600} quantification. OD was
663 quantified using the SpectraMax plate reader and background (determined from blanks) was removed
664 from each quantified sample. Data analysis and visualization of growth during BCAA supplementation
665 was conducted in Excel. To evaluate the relationship between BCAA and c-di-GMP, pure cultures were
666 grown for 24 hours at 30°C and 250 rpm shaking in PMM liquid media containing either 0uM, 50uM,
667 100uM or 150uM of supplemented BCAAs. OD_{600} measurements were taken and samples were diluted
668 to an OD_{600} of 0.04 into PMM at the same BCAA concentrations. Samples were incubated for 24 hours
669 under the same conditions stated and then sonicated (Time 0.00:20, Pulse 01 01, Amplitude 20%) to

670 disrupt cell aggregates. OD_{600} measurements occurred every hour until OD_{600} was approximately equal
671 to 0.25. C-di-GMP analyte extraction was carried out as stated above with the modification that 2mL
672 cultures were used for cell lysis. Quantified values of c-di-GMP are reported as nM/OD_{600} and were
673 visualized with GraphPad Prism9.

674 **Node-edge analysis and visualization**

675 Data reported in Table S1 was used to generate the 'to-from' table which assesses mutation
676 patterns at the gene/protein level (Shannon et al., 2003). Counts were determined by the frequency of
677 the to-from patterns calculated from Table S1 where a mutation in a given gene/protein (to) occurred
678 after a mutation in another gene/protein (from). This table was uploaded to Cytoscape to visualize the
679 nodes (to genes/proteins) and edges (counts). Default renderings of the plot reported node centrality
680 (commonly mutated targets) through coordinate placement on the graph. This metric was converted to
681 node size with larger nodes representing more commonly mutated targets. Nodes were manually
682 aligned for visual clarity with nodes connected by two or more edges being placed in the main ring and
683 nodes with a single edge being placed outside the ring.

684

685 **Supplementary Information**

686 Figures S1-S3 and Tables S1-S3.

687 Table S1 – Source Data 1. BreSeq summary reports of mutations identified in strains isolated in this
688 study.

689

690 **Acknowledgments**

691 We thank RTSF (Michigan State University) for services and assistance with LC-MS/MS analyses and
692 MiGS (Pittsburgh, PA) for services and assistance with whole genome sequencing. This study was funded

693 by the Charles Henry Leach II Fund (W.K.) and the Faculty Development Fund (W.K.) awarded by
694 Duquesne University.
695
696 **Author Contributions**
697 W.K. designed the study, C.K. performed the experiments, C.K and W.K analyzed data and wrote the
698 manuscript.
699
700 **Conflict of Interest**
701 The authors declare no conflict of interest.
702
703 **References**
704 Alexander, R. P., Lowenthal, A. C., Harshey, R. M., & Ottemann, K. M. (2010). CheV: CheW-like coupling
705 proteins at the core of the chemotaxis signaling network. *Trends in Microbiology*, *18*(11), 494–503.
706 https://doi.org/10.1016/j.tim.2010.07.004
707 Armbruster, C. R., Lee, C. K., Parker-Gilham, J., de Anda, J., Xia, A., Zhao, K., Murakami, K., Tseng, B. S.,
708 Hoffman, L. R., Jin, F., Harwood, C. S., Wong, G. C., & Parsek, M. R. (2019). Heterogeneity in surface
709 sensing suggests a division of labor in *Pseudomonas aeruginosa* populations. *ELife*, *8*, 1–29.
710 https://doi.org/10.7554/eLife.45084
711 Bantinaki, E., Kassen, R., Knight, C. G., Robinson, Z., Spiers, A. J., & Rainey, P. B. (2007). Adaptive
712 Divergence in Experimental Populations of *Pseudomonas fluorescens*. III. Mutational Origins of
713 Wrinkly Spreader Diversity. *Genetics*, *176*(1), 441–453.
714 https://doi.org/10.1534/genetics.106.069906

Bellsolell, L., Prieto, J., Serrano, L., & Coll, M. (1994). Magnesium binding to the bacterial chemotaxis protein cheY results in large conformational changes involving its functional surface. In *Journal of Molecular Biology*. https://doi.org/10.1006/jmbi.1994.1308

Borlee, B. R., Goldman, A. D., Murakami, K., Samudrala, R., Wozniak, D. J., & Parsek, M. R. (2010). *Pseudomonas aeruginosa* uses a cyclic-di-GMP-regulated adhesin to reinforce the biofilm extracellular matrix. *Molecular Microbiology*, *75*(4), 827–842. https://doi.org/10.1111/j.1365-2958.2009.06991.x

Buendia, L., Girardin, A., Wang, T., Cottret, L., & Lefebvre, B. (2018). LysM receptor-like kinase and lysM receptor-like protein families: An update on phylogeny and functional characterization. In *Frontiers in Plant Science* (Vol. 871). https://doi.org/10.3389/fpls.2018.01531

Carman, G. M., & Han, G. S. (2006). Roles of phosphatidate phosphatase enzymes in lipid metabolism. In *Trends in Biochemical Sciences* (Vol. 31, Issue 12). https://doi.org/10.1016/j.tibs.2006.10.003

Casarin, R., Facchinetti, A., Sorice, D., & Tonellato, S. (2021). Decision trees and random forests. In *The Essentials of Machine Learning in Finance and Accounting*. https://doi.org/10.4324/9781003037903-2

Chan, C., Paul, R., Samoray, D., Amiot, N., Giese, B., Jenal, U., & Schirmer, T. (2005). Structural basis for the activity and allosteric control of diguanylate cyclase. *Acta Crystallographica Section A Foundations of Crystallography*. https://doi.org/10.1107/s0108767305089993

Chauhan, J. S., Mishra, N. K., & Raghava, G. P. S. (2009). Identification of ATP binding residues of a protein from its primary sequence. *BMC Bioinformatics*, *10*. https://doi.org/10.1186/1471-2105-10-434

Christen, B., Christen, M., Paul, R., Schmid, F., Folcher, M., Jenoe, P., Meuwly, M., & Jenal, U. (2006). Allosteric control of cyclic di-GMP signaling. *Journal of Biological Chemistry*. https://doi.org/10.1074/jbc.M603589200

739 Compeau, G., Al-Achi, B. J., Platsouka, E., & Levy, S. B. (1988). Survival of rifampin-resistant mutants of
740 Pseudomonas fluorescens and Pseudomonas putida in soil systems. *Applied and Environmental*
741 *Microbiology*, *54*(10). https://doi.org/10.1128/aem.54.10.2432-2438.1988
742 Conner, J. G., Zamorano-Sánchez, D., Park, J. H., Sondermann, H., & Yildiz, F. H. (2017). The ins and outs
743 of cyclic di-GMP signaling in Vibrio cholerae. *Current Opinion in Microbiology*, *36*, 20–29.
744 https://doi.org/10.1016/j.mib.2017.01.002
745 Cooley, R. B., Smith, T. J., Leung, W., Tierney, V., Borlee, B. R., O'Toole, G. A., & Sondermann, H. (2016).
746 Cyclic di-GMP-regulated periplasmic proteolysis of a Pseudomonas aeruginosa type Vb secretion
747 system substrate. *Journal of Bacteriology*, *198*(1), 66–76. https://doi.org/10.1128/JB.00369-15
748 Dahlstrom, K. M., Collins, A. J., Doing, G., Taroni, J. N., Gauvin, T. J., Greene, C. S., Hogan, D. A., &
749 O'Toole, G. A. (2018). A multimodal strategy used by a large c-di-GMP network. *Journal of*
750 *Bacteriology*, *200*(8). https://doi.org/10.1128/JB.00703-17
751 Dahlstrom, K. M., Giglio, K. M., Sondermann, H., & O'Toolea, G. A. (2016). The inhibitory site of a
752 diguanylate cyclase is a necessary element for interaction and signaling with an effector protein.
753 *Journal of Bacteriology*, *198*(11), 1595–1603. https://doi.org/10.1128/JB.00090-16
754 De, N., Pirruccello, M., Krasteva, P. V., Bae, N., Raghavan, R. V., & Sondermann, H. (2008).
755 Phosphorylation-Independent Regulation of the Diguanylate Cyclase WspR. *PLoS Biology*, *6*(3), e67.
756 https://doi.org/10.1371/journal.pbio.0060067
757 Edwards, B. D., Greysson-Wong, J., Somayaji, R., Waddell, B., Whelan, F. J., Storey, D. G., Rabin, H. R.,
758 Surette, M. G., & Parkins, M. D. (2017). Prevalence and Outcomes of Achromobacter Species
759 Infections in Adults with Cystic Fibrosis: a North American Cohort Study. *Journal of Clinical*
760 *Microbiology*, *55*(7), 2074–2085. https://doi.org/10.1128/JCM.02556-16

761 Fang, X., Ahmad, I., Blanka, A., Schottkowski, M., Cimdins, A., Galperin, M. Y., Römling, U., & Gomelsky,
762 M. (2014). GIL, a new c-di-GMP-binding protein domain involved in regulation of cellulose
763 synthesis in enterobacteria. *Molecular Microbiology*, *93*(3). https://doi.org/10.1111/mmi.12672
764 Feng, X., Lilly, A. A., & Hazelbauer, G. L. (1999). Enhanced Function Conferred on Low-Abundance
765 Chemoreceptor Trg by a Methyltransferase-Docking Site. *Journal of Bacteriology*, *181*(10), 3164–
766 3171. https://doi.org/10.1128/JB.181.10.3164-3171.1999
767 Giacalone, D., Smith, T. J., Collins, A. J., Sondermann, H., Koziol, L. J., & O'Toole, G. A. (2018). Ligand-
768 mediated biofilm formation via enhanced physical interaction between a diguanylate cyclase and
769 its receptor. *MBio*, *9*(4). https://doi.org/10.1128/mBio.01254-18
770 Giardina, G., Paiardini, A., Fernicola, S., Franceschini, S., Rinaldo, S., Stelitano, V., & Cutruzzolà, F. (2013).
771 Investigating the allosteric regulation of YfiN from Pseudomonas aeruginosa: Clues from the
772 structure of the catalytic domain. *PLoS ONE*, *8*(11). https://doi.org/10.1371/journal.pone.0081324
773 Gloag, E. S., Marshall, C. W., Snyder, D., Lewin, G. R., Harris, J. S., Santos-Lopez, A., Chaney, S. B.,
774 Whiteley, M., Cooper, V. S., & Wozniak, D. J. (2019). *Pseudomonas aeruginosa* interstrain dynamics
775 and selection of hyperbiofilm mutants during a chronic infection. *MBio*, *10*(4), e01698-19.
776 https://doi.org/10.1128/mBio.01698-19
777 Grant, S. S., & Hung, D. T. (2013). Persistent bacterial infections, antibiotic tolerance, and the oxidative
778 stress response. In *Virulence* (Vol. 4, Issue 4). https://doi.org/10.4161/viru.23987
779 Hall, C. L., & Lee, V. T. (2018). Cyclic-di-GMP regulation of virulence in bacterial pathogens. In *Wiley*
780 *Interdisciplinary Reviews: RNA* (Vol. 9, Issue 1). https://doi.org/10.1002/wrna.1454
781 Hengge, R., Galperin, M. Y., Ghigo, J. M., Gomelsky, M., Green, J., Hughes, K. T., Jenal, U., & Landini, P.
782 (2016). Systematic nomenclature for GGDEF and EAL domaincontaining cyclic di-GMP turnover
783 proteins of Escherichia coli. *Journal of Bacteriology*, *198*(1), 7–11.
784 https://doi.org/10.1128/JB.00424-15

785 Huangyutitham, V., Güvener, Z. T., & Harwood, C. S. (2013). Subcellular Clustering of the Phosphorylated
786 WspR Response Regulator Protein Stimulates Its Diguanylate Cyclase Activity. *MBio*, *4*(3), 1–8.
787 https://doi.org/10.1128/mBio.00242-13
788 Huertas-Rosales, Ó., Romero, M., Heeb, S., Espinosa-Urgel, M., Cámara, M., & Ramos-González, M. I.
789 (2017). The Pseudomonas putida CsrA/RsmA homologues negatively affect c-di-GMP pools and
790 biofilm formation through the GGDEF/EAL response regulator CfcR. *Environmental Microbiology*,
791 *19*(9), 3551–3566. https://doi.org/10.1111/1462-2920.13848
792 Irie, Y., Starkey, M., Edwards, A. N., Wozniak, D. J., Romeo, T., & Parsek, M. R. (2010). *Pseudomonas*
793 *aeruginosa* biofilm matrix polysaccharide Psl is regulated transcriptionally by RpoS and post-
794 transcriptionally by RsmA. *Molecular Microbiology*, *78*(1), 158–172.
795 https://doi.org/10.1111/j.1365-2958.2010.07320.x
796 Kessler, C., Mhatre, E., Cooper, V., & Kim, W. (2021). Evolutionary divergence of the Wsp signal
797 transduction system in β- And γ-proteobacteria. *Applied and Environmental Microbiology*, *87*(22).
798 https://doi.org/10.1101/2021.07.02.450980
799 Kim, W., & Levy, S. B. (2008). Increased fitness of Pseudomonas fluorescens Pf0-1 leucine auxotrophs in
800 soil. *Applied and Environmental Microbiology*, *74*(12), 3644–3651.
801 https://doi.org/10.1128/AEM.00429-08
802 Kim, W., Levy, S. B., & Foster, K. R. (2016). Rapid radiation in bacteria leads to a division of labour.
803 *Nature Communications*, *7*(1), 10508. https://doi.org/10.1038/ncomms10508
804 Kirner, S., Krauss, S., Sury, G., Lam, S. T., Ligon, J. M., & van Pée, K. H. (1996). The non-haem
805 chloroperoxidase from Pseudomonas fluorescens and its relationship to pyrrolnitrin biosynthesis.
806 *Microbiology*, *142*(8). https://doi.org/10.1099/13500872-142-8-2129

807 Kuchma, S. L., Delalez, N. J., Filkins, L. M., Snavely, E. A., Armitage, J. P., & O'Toole, G. A. (2015). Cyclic di-
808 GMP-mediated repression of swarming motility by Pseudomonas aeruginosa PA14 Requires the
809 MotAB stator. *Journal of Bacteriology*, *197*(3), 420–430. https://doi.org/10.1128/JB.02130-14
810 Levit, M. N., & Stock, J. B. (2002). Receptor methylation controls the magnitude of stimulus-response
811 coupling in bacterial chemotaxis. *Journal of Biological Chemistry*, *277*(39).
812 https://doi.org/10.1074/jbc.M204325200
813 Li, Y., Hu, Y., Fu, W., Xia, B., & Jin, C. (2007). Solution structure of the bacterial chemotaxis adaptor
814 protein CheW from Escherichia coli. *Biochemical and Biophysical Research Communications*,
815 *360*(4). https://doi.org/10.1016/j.bbrc.2007.06.146
816 Liang, F., Zhang, B., Yang, Q., Zhang, Y., Zheng, D., Zhang, L., Yan, Q., & Wu, X. (2020). Cyclic-di-GMP
817 Regulates the Quorum-Sensing System and Biocontrol Activity of Pseudomonas fluorescens 2P24
818 through the RsmA and RsmE Proteins. *Applied and Environmental Microbiology*, *86*(24).
819 https://doi.org/10.1128/aem.02016-20
820 Liu, J., & Parkinson, J. S. (1991). Genetic evidence for interaction between the CheW and Tsr proteins
821 during chemoreceptor signaling by Escherichia coli. *Journal of Bacteriology*, *173*(16).
822 https://doi.org/10.1128/jb.173.16.4941-4951.1991
823 Malone, J. (2015). Role of small colony variants in persistence of *Pseudomonas aeruginosa* infections in
824 cystic fibrosis lungs. *Infection and Drug Resistance*, *8*, 237–247.
825 https://doi.org/10.2147/IDR.S68214
826 Malone, J. G., Williams, R., Christen, M., Jenal, U., Spiers, A. J., & Rainey, P. B. (2007). The structure–
827 function relationship of WspR, a *Pseudomonas fluorescens* response regulator with a GGDEF
828 output domain. *Microbiology*, *153*(4), 980–994. https://doi.org/10.1099/mic.0.2006/002824-0
829 Mantoni, F., Paiardini, A., Brunotti, P., D'Angelo, C., Cervoni, L., Paone, A., Cappellacci, L., Petrelli, R.,
830 Ricciutelli, M., Leoni, L., Rampioni, G., Arcovito, A., Rinaldo, S., Cutruzzolà, F., & Giardina, G. (2018).

831 Insights into the GTP-dependent allosteric control of c-di-GMP hydrolysis from the crystal structure
832 of PA0575 protein from Pseudomonas aeruginosa. *FEBS Journal*, *285*(20).
833 https://doi.org/10.1111/febs.14634
834 Massie, J. P., Reynolds, E. L., Koestler, B. J., Cong, J.-P., Agostoni, M., & Waters, C. M. (2012).
835 Quantification of high-specificity cyclic diguanylate signaling. *Proceedings of the National Academy*
836 *of Sciences*, *109*(31), 12746–12751. https://doi.org/10.1073/pnas.1115663109
837 Matthews, M., & Roy, C. R. (2000). Identification and subcellular localization of the Legionella
838 pneumophila IcmX protein: A factor essential for establishment of a replicative organelle in
839 eukaryotic host cells. *Infection and Immunity*, *68*(7). https://doi.org/10.1128/IAI.68.7.3971-
840 3982.2000
841 McCarthy, R. R., Mazon-Moya, M. J., Moscoso, J. A., Hao, Y., Lam, J. S., Bordi, C., Mostowy, S., & Filloux,
842 A. (2017). Cyclic-di-GMP regulates lipopolysaccharide modification and contributes to
843 Pseudomonas aeruginosa immune evasion. *Nature Microbiology*, *2*.
844 https://doi.org/10.1038/nmicrobiol.2017.27
845 Merritt, J. H., Brothers, K. M., Kuchma, S. L., & O'Toole, G. A. (2007). SadC reciprocally influences biofilm
846 formation and swarming motility via modulation of exopolysaccharide production and flagellar
847 function. *Journal of Bacteriology*, *189*(22), 8154–8164. https://doi.org/10.1128/JB.00585-07
848 Merritt, J. H., Ha, D. G., Cowles, K. N., Lu, W., Morales, D. K., Rabinowitz, J., Gitai, Z., & O'Toole, G. A.
849 (2010). Specific control of Pseudomonas aeruginosa surface-associated behaviors by two c-di-GMP
850 diguanylate cyclases. *MBio*. https://doi.org/10.1128/mBio.00183-10
851 Monack, D. M., Mueller, A., & Falkow, S. (2004). Persistent bacterial infections: The interface of the
852 pathogen and the host immune system. In *Nature Reviews Microbiology* (Vol. 2, Issue 9).
853 https://doi.org/10.1038/nrmicro955

854 Moscoso, J. A., Jaeger, T., Valentini, M., Hui, K., Jenal, U., & Filloux, A. (2014). The diguanylate cyclase
855 SadC is a central player in Gac/Rsm-mediated biofilm formation in Pseudomonas aeruginosa.
856 *Journal of Bacteriology*, *196*(23), 4081–4088. https://doi.org/10.1128/JB.01850-14
857 Newell, P. D., Yoshioka, S., Hvorecny, K. L., Monds, R. D., & O'Toole, G. A. (2011). Systematic Analysis of
858 Diguanylate Cyclases That Promote Biofilm Formation by *Pseudomonas fluorescens* Pf0-1. *Journal*
859 *of Bacteriology*, *193*(18), 4685–4698. https://doi.org/10.1128/JB.05483-11
860 O'Connor, J. R., Kuwada, N. J., Huangyutitham, V., Wiggins, P. A., & Harwood, C. S. (2012). Surface
861 sensing and lateral subcellular localization of WspA, the receptor in a chemosensory-like system
862 leading to c-di-GMP production. *Molecular Microbiology*, *86*(3), 720–729.
863 https://doi.org/10.1111/mmi.12013
864 Petelski, A. N., & Fonseca Guerra, C. (2019). Designing Self-Assembled Rosettes: Why Ammeline is a
865 Superior Building Block to Melamine. *ChemistryOpen*, *8*(2).
866 https://doi.org/10.1002/open.201800210
867 Ravichandran, A., Ramachandran, M., Suriyanarayanan, T., Wong, C. C., & Swarup, S. (2015). Global
868 regulator MorA affects virulence-associated protease secretion in Pseudomonas aeruginosa PAO1.
869 *PLoS ONE*. https://doi.org/10.1371/journal.pone.0123805
870 Re, S. da, Tolstykh, T., Wolanin, P. M., & Stock, J. B. (2002). Genetic analysis of response regulator
871 activation in bacterial chemotaxis suggests an intermolecular mechanism. *Protein Science*, *11*(11),
872 2644–2654. https://doi.org/10.1110/ps.0220402
873 Reichhardt, C., Wong, C., da Silva, D. P., Wozniak, D. J., & Parsek, M. R. (2018). CDRA interactions within
874 the pseudomonas aeruginosa biofilm matrix safeguard it from proteolysis and promote cellular
875 packing. *MBio*, *9*(5). https://doi.org/10.1128/mBio.01376-18

Ricca, E., Limauro, D., Lago, C. T., & de Felice, M. (1988). Enhanced acetohydroxy acid synthase III activity in an ilvH mutant of Escherichia coli K-12. *Journal of Bacteriology*, *170*(11). https://doi.org/10.1128/jb.170.11.5197-5199.1988

Rice, M. S., & Dahlquist, F. W. (1991). Sites of deamidation and methylation in Tsr, a bacterial chemotaxis sensory transducer. *Journal of Biological Chemistry*, *266*(15), 9746–9753. https://doi.org/10.1016/S0021-9258(18)92884-X

Römling, U., Galperin, M. Y., & Gomelsky, M. (2013). Cyclic di-GMP: the First 25 Years of a Universal Bacterial Second Messenger. *Microbiology and Molecular Biology Reviews*, *77*(1), 1–52. https://doi.org/10.1128/MMBR.00043-12

Sarenko, O., Klauck, G., Wilke, F. M., Pfiffer, V., Richter, A. M., Herbst, S., Kaever, V., & Hengge, R. (2017). More than enzymes that make or break cyclic Di-GMP—local signaling in the interactome of GGDEF/EAL domain proteins of Escherichia coli. *MBio*, *8*(5). https://doi.org/10.1128/mBio.01639-17

Schumacher, M. A., Gallagher, K. A., Holmes, N. A., Chandra, G., Henderson, M., Kysela, D. T., Brennan, R. G., & Buttner, M. J. (2021). Evolution of a σ–(c-di-GMP)–anti-σ switch. *Proceedings of the National Academy of Sciences of the United States of America*, *118*(30). https://doi.org/10.1073/pnas.2105447118

Shannon, P., Markiel, A., Ozier, O., Baliga, N. S., Wang, J. T., Ramage, D., Amin, N., Schwikowski, B., & Ideker, T. (2003). Cytoscape: A software Environment for integrated models of biomolecular interaction networks. *Genome Research*, *13*(11). https://doi.org/10.1101/gr.1239303

Skotnicka, D., Petters, T., Heering, J., Hoppert, M., Kaever, V., & Søgaard-Andersen, L. (2016). Cyclic dI-GMP regulates type IV pilus-dependent motility in Myxococcus xanthus. *Journal of Bacteriology*, *198*(1). https://doi.org/10.1128/JB.00281-15

899 Soto, S. M. (2013). Role of efflux pumps in the antibiotic resistance of bacteria embedded in a biofilm.
900 *Virulence*, *4*(3). https://doi.org/10.4161/viru.23724
901 Spiers, A. J., Kahn, S. G., Bohannon, J., Travisano, M., & Rainey, P. B. (2002). Adaptive divergence in
902 experimental populations of *Pseudomonas fluorescens*. I. Genetic and phenotypic bases of wrinkly
903 spreader fitness. *Genetics*, *161*, 33–46.
904 Starkey, M., Hickman, J. H., Ma, L., Zhang, N., de Long, S., Hinz, A., Palacios, S., Manoil, C., Kirisits, M. J.,
905 Starner, T. D., Wozniak, D. J., Harwood, C. S., & Parsek, M. R. (2009). *Pseudomonas aeruginosa*
906 Rugose Small-Colony Variants Have Adaptations That Likely Promote Persistence in the Cystic
907 Fibrosis Lung. *Journal of Bacteriology*, *191*(11), 3492–3503. https://doi.org/10.1128/JB.00119-09
908 Tamayo, R. (2019). Cyclic diguanylate riboswitches control bacterial pathogenesis mechanisms. *PLoS*
909 *Pathogens*, *15*(2). https://doi.org/10.1371/journal.ppat.1007529
910 Wassmann, P., Chan, C., Paul, R., Beck, A., Heerklotz, H., Jenal, U., & Schirmer, T. (2007). Structure of
911 BeF3--Modified Response Regulator PleD: Implications for Diguanylate Cyclase Activation,
912 Catalysis, and Feedback Inhibition. *Structure*. https://doi.org/10.1016/j.str.2007.06.016
913 Wehbi, H., Portillo, E., Harvey, H., Shimkoff, A. E., Scheurwater, E. M., Howell, P. L., & Burrows, L. L.
914 (2011). The peptidoglycan-binding protein fimv promotes assembly of the pseudomonas
915 aeruginosa type IV pilus secretin. *Journal of Bacteriology*, *193*(2).
916 https://doi.org/10.1128/JB.01048-10
917 Wei, Q., Leclercq, S., Bhasme, P., Xu, A., Zhu, B., Zhang, Y., Zhang, M., Wang, S., & Maa, L. Z. (2019).
918 Diguanylate cyclases and phosphodiesterases required for basal-level c-di-GMP in Pseudomonas
919 aeruginosa as revealed by systematic phylogenetic and transcriptomic analyses. *Applied and*
920 *Environmental Microbiology*, *85*(21). https://doi.org/10.1128/AEM.01194-19

921 Yan, J., Deforet, M., Boyle, K. E., Rahman, R., Liang, R., Okegbe, C., Dietrich, L. E. P., Qiu, W., & Xavier, J.
922 B. (2017). Bow-tie signaling in c-di-GMP: Machine learning in a simple biochemical network. *PLOS*
923 *Computational Biology*, *13*(8), e1005677. https://doi.org/10.1371/journal.pcbi.1005677

924

925 **Figure Legends**

926 **Figure 1. Bidirectional evolution of M and D phenotypes are c-di-GMP dependent.** A) Colony
927 morphologies of the ancestral mucoid (M, left) and dry (D, middle) strains after 4 days of growth. Arrows
928 indicate the emergence of spreading fans that contain the respective parent strain and a new mutant
929 strain with the opposite phenotype. The spreading phenotype is readily produced by artificially mixing M
930 and D strains (right, scale bar = 10mm). B) Phylogeny of strains in select lineages colored by phenotype
931 and corresponding colony morphologies are shown in Fig. S2. The numbers indicate the IDs of the
932 evolved strains as shown in Table S1. Each strain was isolated from naturally emerging fans from their
933 respective parent colony with the opposite phenotype. This phylogeny depicts the bidirectional
934 transitions between mucoid and dry states which we show are c-di-GMP dependent. C) C-di-GMP levels
935 of evolved strains. C-di-GMP was quantified through LC-MS/MS and is reported as nM per OD600.
936 Samples are categorized by phenotype and we report the triplicate mean ± SD for each phenotypic
937 classification: mucoid n=14 and dry n=21 (*** Student's t-test $p < 0.001$).

938

939 **Figure 2. Functional model of the Wsp signal transduction system.** The Wsp system in *P. aeruginosa*
940 responds to surface contact to ultimately produce c-di-GMP. (CH3 = methyl group, P= phosphoryl
941 group).

942

943 **Figure 3. C-di-GMP oscillates between all M and D phenotypic transitions.** C-di-GMP was quantified via
944 LC-MS/MS and is reported as the triplicate mean ± SD. The charts capture the independently evolved

945 strains within the five selected lineages shown in Figure 1B. D strains are shown in orange and M strains
946 are shown in blue. The numerical IDs correspond to Table S1, and mutations reflect the affected amino
947 acid residues, except frameshift (FS) and promoter region (PR) mutations refer to the specific
948 nucleotides.
949
950 **Figure 4. C-di-GMP levels fluctuate with BCAA mutations.** C-di-GMP measurements in triplicate mean ±
951 SD. Raw c-di-GMP values of each mutant and its respective parent are reported in Table S1. Causal
952 mutation of each phenotypic shift is indicated on the left. D strains are shown in orange and M strains
953 are shown in blue. (Student's t-test: ns = non-significant, * = $p < 0.05$).
954
955 **Figure 5. BCAA supplementation stimulates c-di-GMP production in a BCAA auxotroph with the M**
956 **phenotype, but does not impact c-di-GMP production in non-BCAA auxotrophs with the same M**
957 **phenotype.** Strains were grown in the chemically defined PMM medium with 0, 50, 100, or 150 uM
958 BCAA supplementation (valine, leucine, isoleucine). C-di-GMP was extracted and quantified via LC-
959 MS/MS in triplicates and plotted as the mean with STD (ANOVA; Tukey's HSD Post Test: ns = non-
960 significant, * = $p < 0.05$). M and D refer to the prototypical M and D strains in Fig. 1A. The *ilvH* mutant (D
961 strain 5.7) produces c-di-GMP levels similar to the D strain control and the *parA* mutant (M strain 5.8)
962 produces c-di-GMP levels similar to the M strain control. These relative patterns are consistent with the
963 c-di-GMP quantification data reported in Fig 4 under nutrient-rich conditions. Exogenous
964 supplementation of BCAA across all concentrations does not significantly impact c-di-GMP production.
965 There is no data for the *ilvI* mutant at 0 uM BCAA, since this strain fails to grow in PMM unless BCAA is
966 exogenously provided. However, the *ilvI* mutant (M strain 5.10a) produces c-di-GMP levels comparable
967 to both D and the *ilvH* mutant (D strain 5.7) with BCAA supplementation.
968

969 **Figure 6. A node-edge representation of 147 unique mutations across 33 lineages and c-di-GMP**
970 **quantification data of strains with mutations in proteins with significant network connectivity that are**
971 **not known to be associated with c-di-GMP modulation.** A) A node-edge plot reveals focal proteins
972 under selection. Each node represents a protein and each edge represents a relationship where one
973 mutation precedes or proceeds another. Orange edges represent M to D shifts and blue edges represent
974 D to M shifts. The relative size of a node and thickness of an edge is proportional to frequencies within
975 the dataset. Proteins that collectively form the ring represent commonly mutated targets in this study
976 and likely have a substantial role in c-di-GMP regulation. Proteins with limited connectivity fall outside
977 the main ring. B) LC-MS/MS validates that proteins with significant network connectivity, but not
978 previously associated with c-di-GMP, have a significant impact on intracellular c-di-GMP levels. C-di-
979 GMP measurements are reported as the triplicate mean ± SD. C-di-GMP values of each mutant and its
980 respective parent are summarized in Table S1 with the corresponding ID tag. D strains are shown in
981 orange and M strains are shown in blue. (Student's t-test: * = $p < 0.05$, ** = $p < 0.01$).
982
983 **Table S1 – Source Data 1. BreSeq summary reports of mutations identified in strains isolated in this**
984 **study.** Whole genome sequencing data of select strains from the parallel evolution experiments were
985 subjected to variant analysis using the BreSeq algorithm against the published *P. fluorescens* Pf0-1
986 genome sequence. Summary files are provided for each analysis where the 'Strain ID' reported in Table
987 S1 is represented as the file name.
988
989
990
991
992

Table 1. Reconstructing select naturally acquired mutations in both the ancestral and direct parent strains reveal dependence on the previous mutation(s) to drive specific M-D phenotypic shifts.

Strain ID	Strain Mutation	Mutation CDS ID	Mutant Phenotype	Parent Strain ID	Parent Strain Mutation	Ancestor ‡	Reconstructed Mutants*	
							Parent	Ancestor
5.9a	WspA::D	Pfl01_1052::1055	dry	5.8a	ParA (D115N)	M	dry	mucoid
5.9b	WspB::D	Pfl01_1053::1055	dry	5.8a	ParA (D115N)	M	dry	mucoid
30.1	WspC::D	Pfl01_1054::1055	dry	Δ*rsmE*	Δ*rsmE*	M	dry	dry
27.3b	IlvH (A36E)	Pfl01_4787	dry	27.2	DcgH (Q148P)	M	dry	mucoid
5.7a	IlvH (S149R)	Pfl01_4787	dry	5.6a	SadC (25L 4→3)	M	dry	mucoid
5.9e	IlvH (G150S)	Pfl01_4787	dry	5.8b	YfiN (I212T)	M	dry	mucoid
5.10b	IlvI (Δ17bp)	Pfl01_4788	mucoid	5.9b	WspB::D	D	mucoid	dry
5.10a	IlvI (Δ 23bp)	Pfl01_4788	mucoid	5.9b	WspB::D	D	mucoid	dry
6.5a	DgcY (Δ3505-3506)	Pfl01_3505-3506	dry	6.4	WspE (+1bp)	M	dry	mucoid
6.6a	DgcY (Δ3500-3510)	Pfl01_3500-3510	mucoid	6.5a	DgcY (Δ3505-3506)	D	mucoid	dry
2.3	NarA (A383S)	Pfl01_3147	dry	2.2	WspD (W90L)	M	dry	mucoid
10.2	CalM (+5bp)	Pfl01_1895	mucoid	10.1	DgcH (Δ467-470)	D	mucoid	dry
11.2	RndA (Q51S)	Pfl01_2749	mucoid	11.1	WspA (A381V)	D	mucoid	dry
6.8a	CdrB (A290T)	Pfl01_0652	mucoid	6.7c	YfiN (G157C)	D	mucoid	dry

‡ Ancestors are the prototype M or D strains (Fig. 1).
* Each mutation was reconstructed in the direct parent and the corresponding ancestor strain. WGS confirmed the reconstruction of each mutation.

993

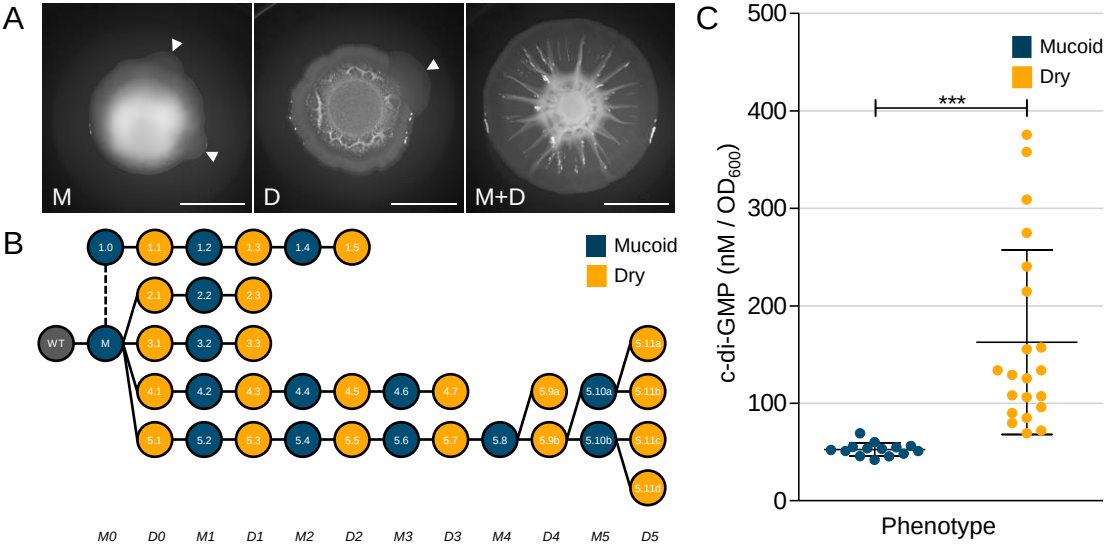
A
M
D
M+D
B
Mucoid
Dry
WT
M
1.0
1.1
1.2
1.3
1.4
1.5
2.1
2.2
2.3
3.1
3.2
3.3
4.1
4.2
4.3
4.4
4.5
4.6
4.7
5.1
5.2
5.3
5.4
5.5
5.6
5.7
5.8
5.9a
5.9b
5.10a
5.10b
5.11a
5.11b
5.11c
5.11d
M0
D0
M1
D1
M2
D2
M3
D3
M4
D4
M5
D5
C
Mucoid
Dry
***
c-di-GMP (nM / OD600)
500
400
300
200
100
0
Phenotype

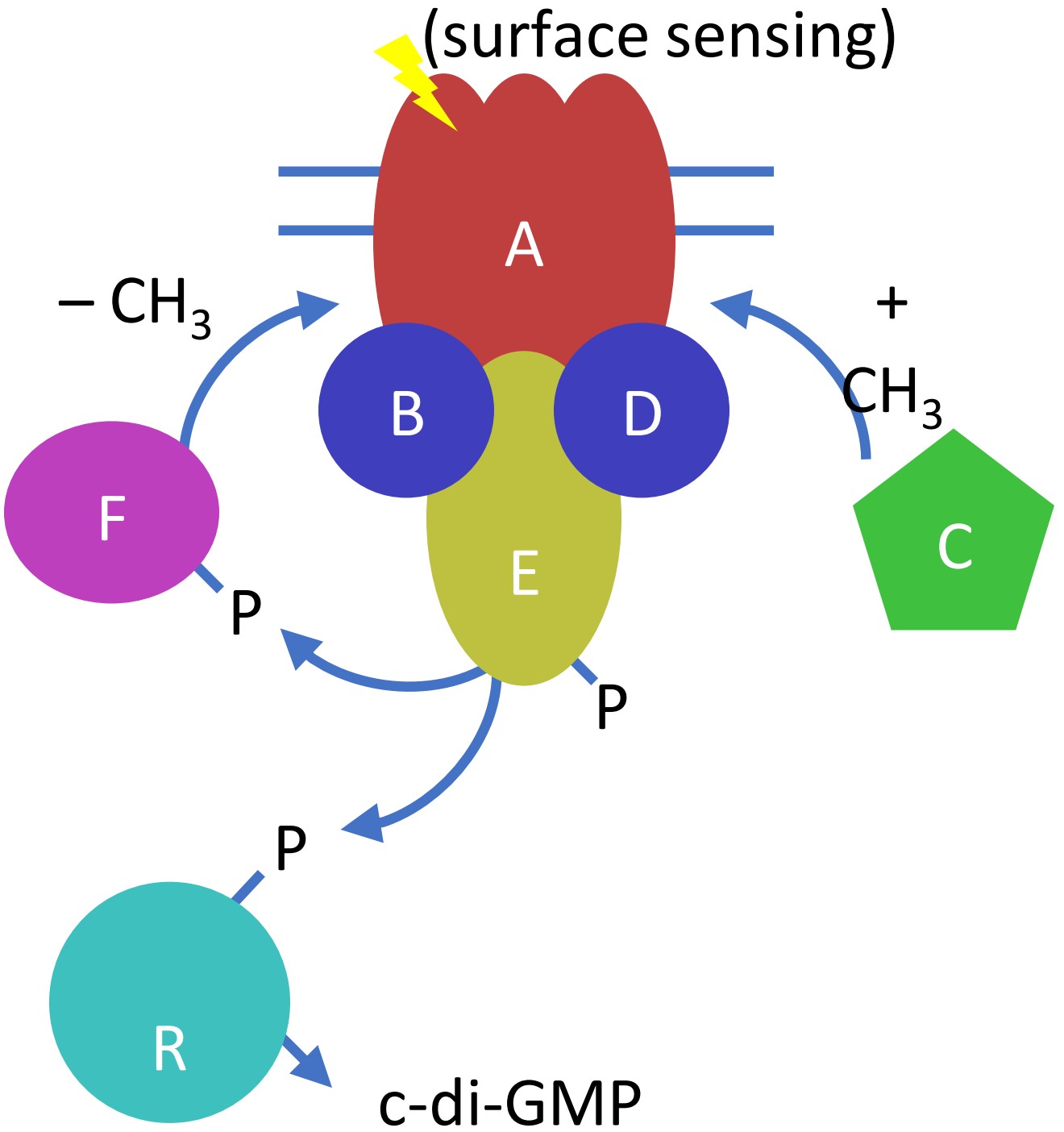
(surface sensing)
A
– CH_3
+
CH_3
B
D
F
C
E
P
P
P
R
c-di-GMP

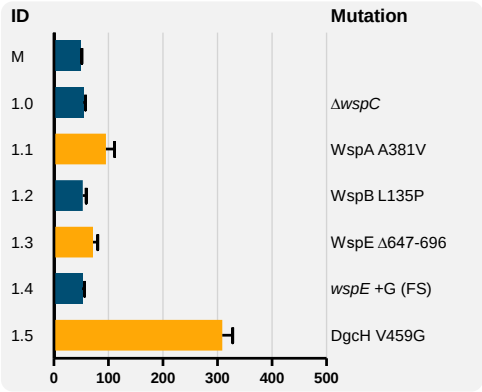
ID
Mutation
M
1.0
Δ*wspC*
1.1
WspA A381V
1.2
WspB L135P
1.3
WspE Δ647-696
1.4
wspE +G (FS)
1.5
DgcH V459G
0
100
200
300
400
500

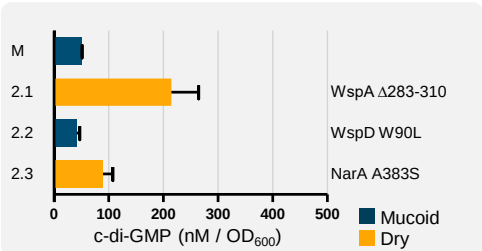
M
2.1
WspA Δ283-310
2.2
WspD W90L
2.3
NarA A383S
0
100
200
300
400
500
c-di-GMP (nM / OD600)
Mucoid
Dry

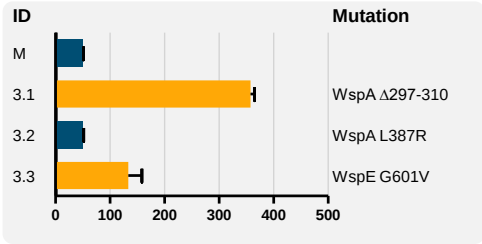
ID
Mutation
M
3.1
WspA Δ297-310
3.2
WspA L387R
3.3
WspE G601V
0
100
200
300
400
500

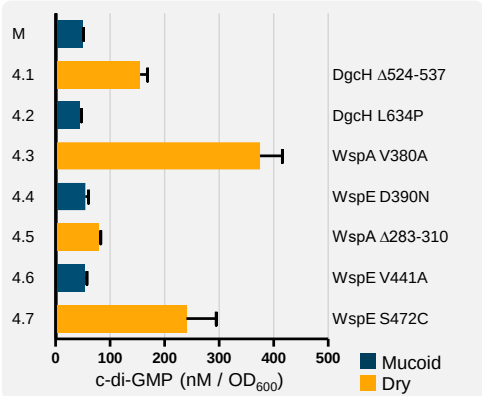
M
4.1
DgcH Δ524-537
4.2
DgcH L634P
4.3
WspA V380A
4.4
WspE D390N
4.5
WspA Δ283-310
4.6
WspE V441A
4.7
WspE S472C
0
100
200
300
400
500
c-di-GMP (nM / OD600)
Mucoid
Dry

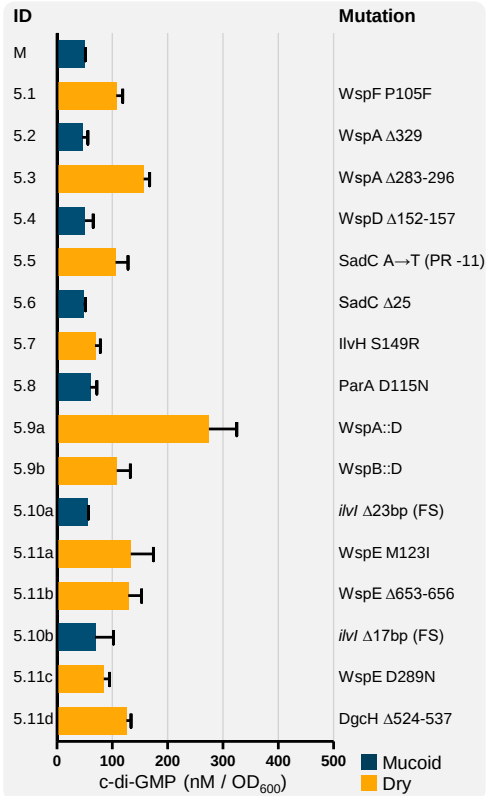
ID
Mutation
M
5.1
WspF P105F
5.2
WspA Δ329
5.3
WspA Δ283-296
5.4
WspD Δ152-157
5.5
SadC A→T (PR -11)
5.6
SadC Δ25
5.7
IlvH S149R
5.8
ParA D115N
5.9a
WspA::D
5.9b
WspB::D
5.10a
ilvI Δ23bp (FS)
5.11a
WspE M123I
5.11b
WspE Δ653-656
5.10b
ilvI Δ17bp (FS)
5.11c
WspE D289N
5.11d
DgcH Δ524-537
0
100
200
300
400
500
c-di-GMP (nM / OD600)
Mucoid
Dry

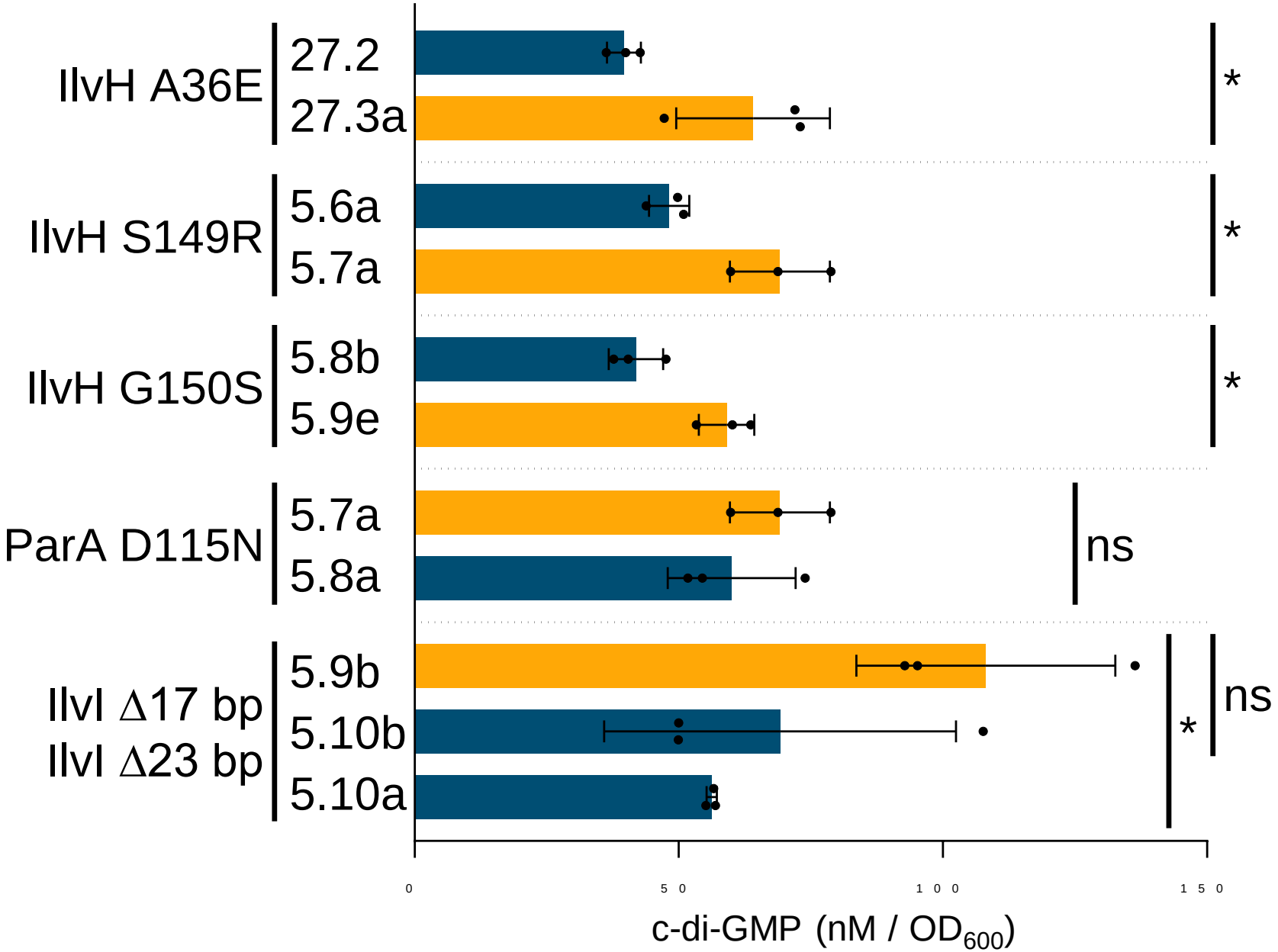
IlvH A36E
27.2
27.3a
*
IlvH S149R
5.6a
5.7a
*
IlvH G150S
5.8b
5.9e
*
ParA D115N
5.7a
5.8a
ns
IlvI Δ17 bp
IlvI Δ23 bp
5.9b
5.10b
5.10a
*
ns
0
50
100
150
c-di-GMP (nM / OD600)

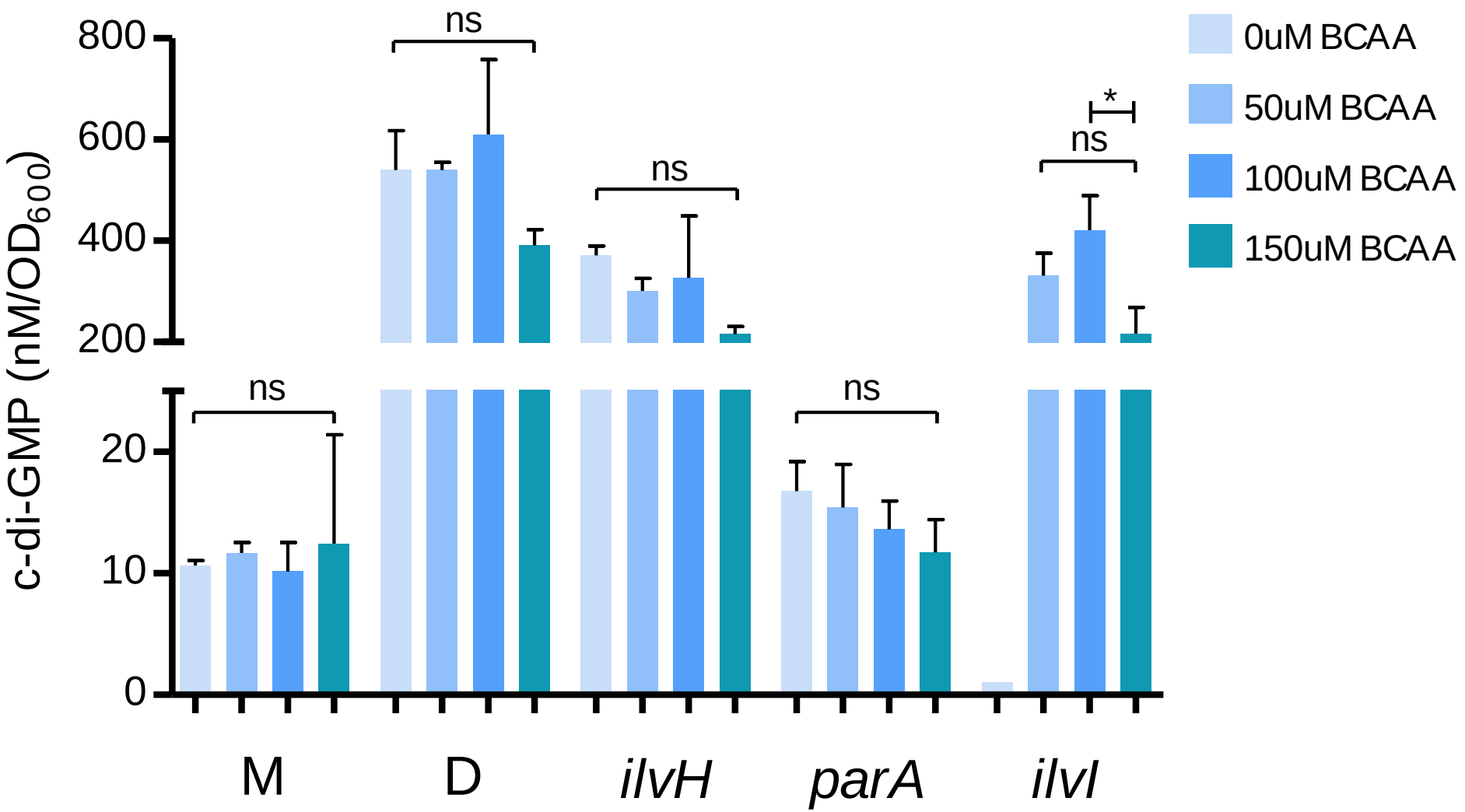
c-di-GMP (nM/OD600)
800
600
400
200
20
10
0
ns
ns
ns
ns
*
ns
0uM BCAA
50uM BCAA
100uM BCAA
150uM BCAA
M
D
ilvH
parA
ilvI

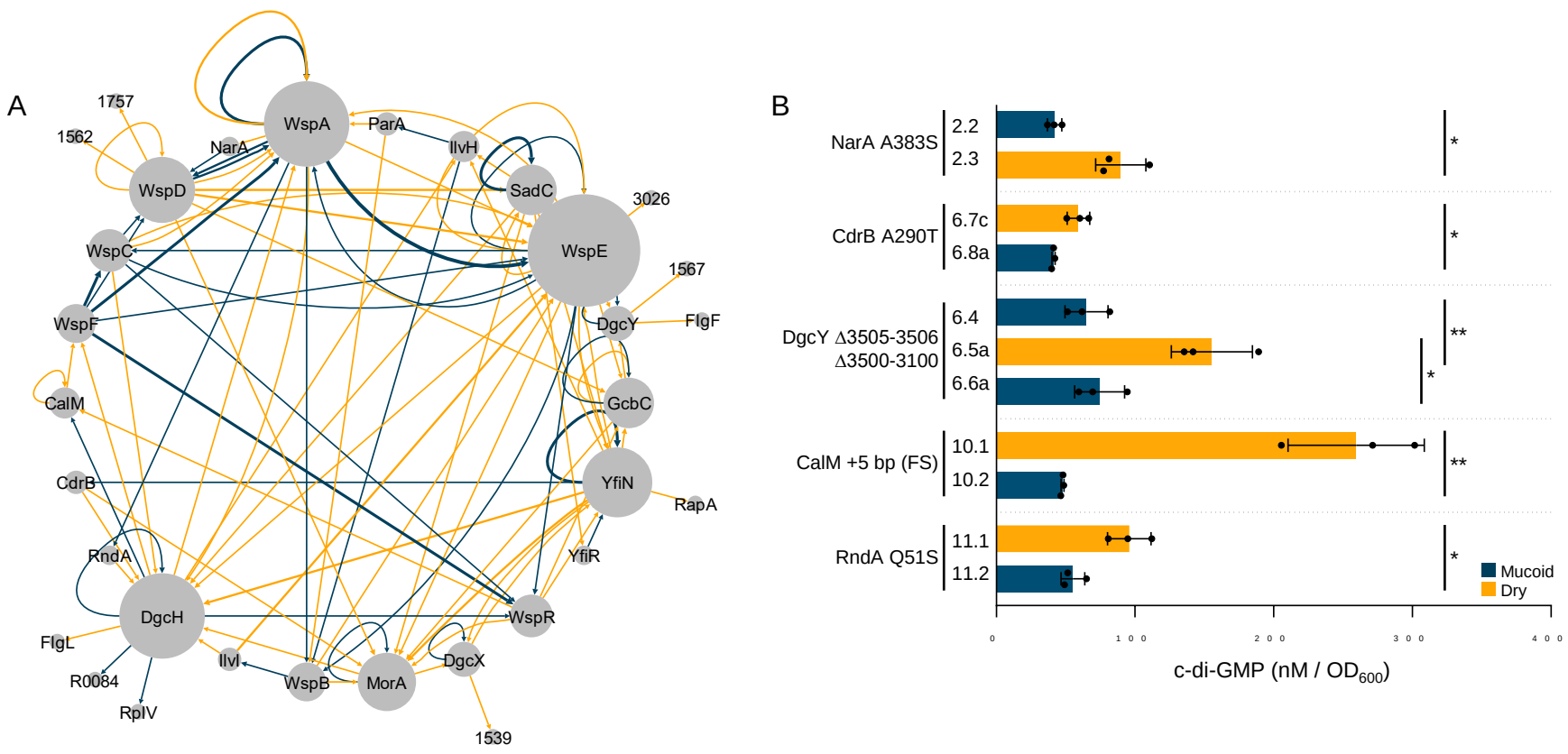
A
1757
1562
WspA
ParA
NarA
IlvH
WspD
SadC
3026
WspC
WspE
1567
WspF
DgcY
FlgF
CalM
GcbC
CdrB
YfiN
RapA
RndA
YfiR
DgcH
WspR
FlgL
IlvI
DgcX
R0084
WspB
MorA
RpIV
1539
B
NarA A383S
2.2
2.3
CdrB A290T
6.7c
6.8a
DgcY Δ3505-3506
Δ3500-3100
6.4
6.5a
6.6a
CalM +5 bp (FS)
10.1
10.2
RndA Q51S
11.1
11.2
Mucoid
Dry
0
100
200
300
400
c-di-GMP (nM / OD600)

Global characterization of the cyclic-di-GMP regulome by bi-directionally evolving a social trait in *Pseudomonas fluorescens*

Collin Kessler[1], Wook Kim[1*]

[1] Department of Biological Sciences, Duquesne University, Pittsburgh, PA 15101, USA

*** Correspondence:**
kimw1@duq.edu

Supplemental Figures

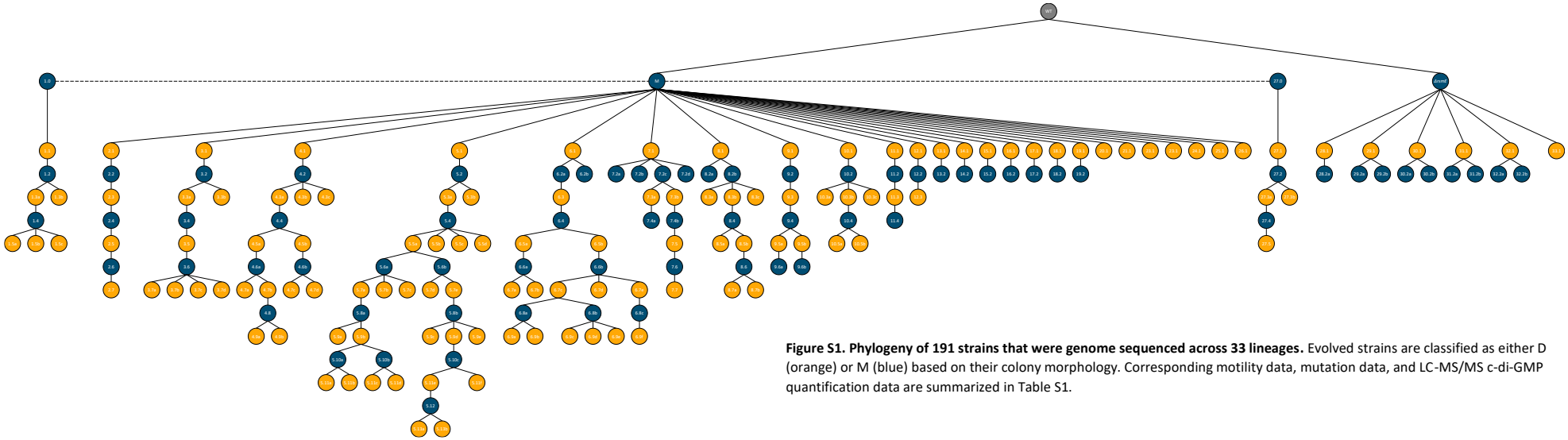

Figure S1. Phylogeny of 191 strains that were genome sequenced across 33 lineages. Evolved strains are classified as either D (orange) or M (blue) based on their colony morphology. Corresponding motility data, mutation data, and LC-MS/MS c-di-GMP quantification data are summarized in Table S1.

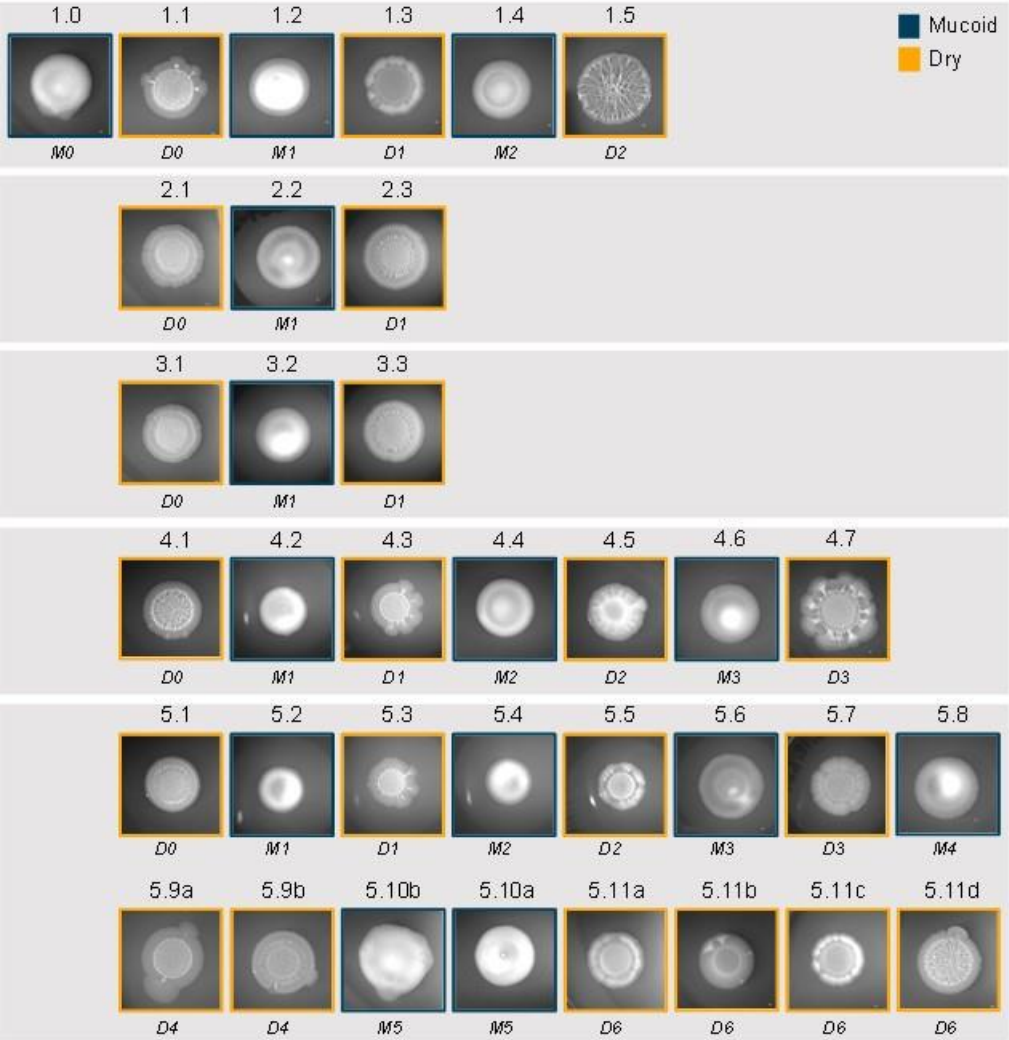

Figure S2. Colony morphologies of evolved strains depicted in Fig. 1B. Each evolved strain is classified either as M (blue) or D (orange) based on their mucoid or dry-wrinkly colony phenotypes, respectively. Motility data and LC-MS/MS c-di-GMP quantification data for each strain are reported in Table S1.

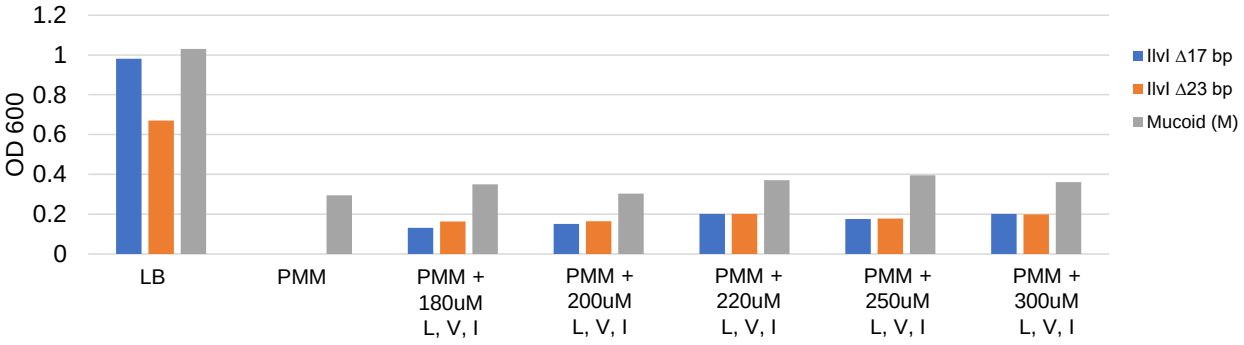

Figure S3. *ilvI* mutants require exogenous supplementation of BCAA. The ancestral M and independently isolated *ilvI* mutant strains were grown in LB (nutrient-rich medium) or PMM (minimal medium) with or without exogenous BCAA supplementation. Both *ilvI* mutants fail to grow in PMM unless supplied with BCAA (leucine (L), valine (V), and isoleucine (I)), and M does not show substantial change in growth with BCAA supplementation.

14

15

Table S1. 191 strains isolated from the parallel evolution experiment categorized by lineage.

Strain ID §	Generation §§	Motility Assay †	LC-MS/MS (nM/OD 600) ‡			Locus ***	CDS ID ***	Mutation Location (NT) ***	Consequence ***	Genotype (AA) ***	Genotype (NT) ***
			Replicate A	Replicate B	Replicate C						
WT #	WT	motile	59.23	73.16	62.21	na	na	na	na	na	na
M *	M0	motile	49.19	51.54	48.64	RsmE	Pfl01_1912 ←	2186046	Frame shift	Frame shift	Δ1 bp 126/195 nt
D **	D0	non-motile	187.52	146.52	156.37	WspC	Pfl01_1054 →	1222594	In-frame readthrough	In-frame readthrough	Δ2 bp 1269-1270/1278 nt
1.0 **	M0	motile	49.64	58.15	53.51	WspC	Pfl01_1054 →	1221330	In-frame Δ	Δ*wspC*	Δ5-1278/1278 nt
1.1	D0	non-motile	80.66	94.75	112.01	WspA	Pfl01_1052 →	1220312	Missense	A381V	GCC→GTC
1.2	M1	motile	52.28	59.70	47.26	WspB	Pfl01_1053 →	1221196	Missense	L135P	CTG→CCG
1.3a	D1	non-motile	63.54	81.09	71.31	WspE	Pfl01_1056 →	1225308	In-frame Δ	Δ674-696	Δ2029-2097/2295 nt
1.3b	D1	non-motile				WspE	Pfl01_1056 →	1225307	Duplication	673GMD 1→2	+9bp 2028/2295 nt
1.4	M2	motile	56.99	49.71	49.42	WspE	Pfl01_1056 →	1224117	Frame shift	289*	+1bp 838/2295
1.5a	D2	non-motile	290.55	328.67	307.72	DgcH	Pfl01_0050 ←	55870	Missense	V459G	GTC→GGC
1.5b	D2	non-motile				DgcH	Pfl01_0050 ←	55317	Duplication	+472-643 @ 643	+513bp 1929/2091 nt
1.5c	D2	non-motile				Pfl01_3026	Pfl01_3026 →	3463653	Missense	T242I	ACC→ATC
2.1	D0	non-motile	167.26	267.13	209.38	WspA	Pfl01_1052 →	1220020	In-frame Δ	Δ283-310	Δ850-933/1623 nt
2.2	M1	motile	47.27	41.65	36.89	WspD	Pfl01_1055 →	1222868	Missense	W90L	TGG→TTG
2.3	D1	non-motile	77.37	81.28	110.54	NarA	Pfl01_3147 →	3613968	Missense	A383S	GCC→TCC
2.4	M2	motile				WspD	Pfl01_1055 →	1223197	Nonsense	R200*	CGA→TGA
2.5	D2	non-motile				GcbC	Pfl01_4665 →/ → Pfl01_4666	5266677	5' UTR	+ Pfl01_2031-2032	+1316 +54/-56
2.6	M3	motile				WspA	Pfl01_1052 →	1219276	Nonsense	E36*	GAA→TAA
2.7	D3	non-motile				DgcH	Pfl01_0050 ←	55909	In-frame Δ	Δ441-446	Δ15bp 1323-1337/2091 nt
3.1	D0	non-motile	349.34	359.63	363.90	WspA	Pfl01_1052 →	1220059	In-frame Δ	Δ297-310	Δ889-930/1623 nt
3.2	M1	motile	49.45	51.62	51.41	WspA	Pfl01_1052 →	1220330	Missense	L387R	CTG→CGG
3.3a	D1	non-motile	127.36	112.64	160.92	WspE	Pfl01_1056 →	1225081	Missense	G601V	GGC→GTC
3.3b	D1	non-motile				WspE	Pfl01_1056 →	1224300	Missense	E341K	GAA→AAA
3.4	M2	motile				WspR	Pfl01_1058 →	1227186	Missense	L186Q	CTG→CAG
3.5	D2	non-motile				YfiN	Pfl01_0692 →	818804	Missense	G157A	GGT→GCT
3.6	M3	motile				YfiN	Pfl01_0692 →	819473	In-frame Δ	Δ381-385	Δ1139-1153/1269 nt
3.7a	D3	non-motile				DgcX	Pfl01_3550 →	4023270	Missense	M350I	ATG→ATA
3.7b	D3	non-motile				GcbC	Pfl01_4665 →/ → Pfl01_4666	5266677	5' UTR	+ Pfl01_2031-2032	+1316 +54/-56
3.7c	D3	non-motile				MorA	Pfl01_4876 →	5499015	Missense	M991T	ATG→ATA
3.7d	D3	non-motile				MorA	Pfl01_4876 →	5499101	Missense	A1020E	GCG→GAG
4.1	D0	non-motile	145.66	170.85	148.76	DgcH	Pfl01_0050 ←	55647	In-frame Δ	Δ524-537	Δ1558-1599/2091 nt
4.2	M1	motile	42.78	46.36	47.13	DgcH	Pfl01_0050 ←	55345	Missense	L634P	CTC→CCC
4.3a	D1	non-motile	392.53	328.69	404.68	WspA	Pfl01_1052 →	1220309	Missense	V380A	GTC→GCC
4.3b	D1	non-motile				WspF	Pfl01_1057 →	1226046	Missense	S159L	TCG→TTG
4.3c	D1	non-motile				WspA	Pfl01_1052 →	1220170	In-frame Δ	Δ334-336	Δ1000-1008/1623 nt
4.4	M2	motile	50.14	53.49	61.31	WspE	Pfl01_1056 →	1224447	Missense	D390N	GAC→AAC
4.5a	D2	non-motile	81.95	81.25	75.76	WspA	Pfl01_1052 →	1220020	In-frame Δ	Δ283-310	Δ850-933/1623 nt
4.5b	D2	non-motile				WspA	Pfl01_1052 →	1219961	Missense	Q264L	CAG→CTG
4.6a	M3	motile	57.50	54.72	51.88	WspE	Pfl01_1056 →	1224601	Missense	V441A	GTG→GCG
4.6b	M3	motile	54.52	56.68	55.08	WspD	Pfl01_1055 →	1223058	In-frame Δ	Δ152-157	Δ459-476/684 nt
4.7a	D3	non-motile	275.45	268.03	177.32	WspE	Pfl01_1056 →	1224693	Missense	S472C	AGT→TGT
4.7b	D3	non-motile				GcbC	Pfl01_4665 →/ → Pfl01_4666	5266677	5' UTR	+ Pfl01_2031-2032	+1316 +54/-56
4.7c	D3	non-motile				FleN	Pfl01_1562 →	1752356	Missense	T13I	ACC→ATC
4.7d	D3	non-motile				CysH	Pfl01_1757 ←	1952544	Nonsense	W51*	TGG→TGA
4.8	M4	motile				GcbC	Pfl01_4666 →	5268046	Frame shift	Frame shift	+1bp 1314/1506 nt
4.9a	D4	non-motile				DgcY	Pfl01_3502	3982758	Frame shift	Frame shift	Δ502-555/672 nt
4.9b	D4	non-motile				MorA	Pfl01_4876 →	5498817	Missense	M925I	ATG→ATC
5.1	D0	non-motile	106.41	95.85	119.21	WspF	Pfl01_1057 →	1225883	Missense	P105S	CCG→TCG
5.2	M1	motile	39.11	39.97	57.53	WspA	Pfl01_1052 →	1220156	In-frame Δ	Δ329	Δ986-988/1623 nt
5.3a	D1	non-motile	158.40	145.92	166.92	WspA	Pfl01_1052 →	1220017	In-frame Δ	Δ283-296	Δ847-888/1623 nt
5.3b	D1	non-motile				WspA	Pfl01_1052 →	1220020	In-frame Δ	Δ283-310	Δ850-933/1623 nt
5.4	M2	motile	40.20	67.63	44.65	WspD	Pfl01_1055 →	1223058	In-frame Δ	Δ152-157	Δ459-476/684 nt
5.5a	D2	non-motile	131.86	92.83	93.92	SadC	Pfl01_4451 ←	5013023	5' UTR	5' UTR	A→T (-11)
5.5b	D2	non-motile				SadC	Pfl01_4451 ←	5013023	5' UTR	5' UTR	A→C (-11)
5.5c	D2	non-motile				SadC	Pfl01_4451 ←	5013023	5' UTR	5' UTR	A→C (-11)
5.5d	D2	non-motile				WspE	Pfl01_1056 →	1224211	Duplication	308RMV 1→2	+9bp 932/2295
5.6a	M3	motile	49.79	50.94	43.86	SadC	Pfl01_4451 ←	5012937	In-frame Δ	25L 4→3	Δ74-76/1107 nt
5.6b	M3	motile				SadC	Pfl01_4451 ←	5012937	In-frame Δ	25L 4→3	Δ74-76/1107 nt
5.7a	D3	non-motile	68.79	59.84	78.79	IlvH	Pfl01_4787 ←	5402643	Missense	S149R	AGT→AGG
5.7b	D3	non-motile				DgcH	Pfl01_0050 ←	55647	In-frame Δ	Δ524-537	Δ1558-1599/2091 nt
5.7c	D3	non-motile				WspE	Pfl01_1056 →	1225351	Missense	D691G	GAC→GGC
5.7d	D3	non-motile				WspE	Pfl01_1056 →	1224324	Missense	R349S	CGC→AGC
5.7e	D3	non-motile				YfiN	Pfl01_0692 →	818804	Missense	G157A	GGT→GCT
5.8a	M4	motile	54.44	51.70	73.94	ParA	Pfl01_0730 →	858438	Missense	D115N	GAT→AAT
5.8b	M4	motile	47.61	37.67	40.41	YfiN	Pfl01_0692 →	818969	Missense	I212T	ATT→ACT
5.9a	D4	non-motile	329.69	230.96	263.57	WspA	Pfl01_1052 →	1220649	In-frame Δ	wspA::D	Δ2421 bp
5.9b	D4	non-motile	92.77	95.21	136.41	WspB	Pfl01_1053 →	1220923	In-frame Δ	wspB::D	Δ1840 bp
5.9c	D4	non-motile				WspE	Pfl01_1056 →	1223451	Missense	R58W	CGG→TGG

5.9d	D4	non-motile				WspE	Pfl01_1056 →	1223648	Missense	M123I	ATG→ATA
5.9e	D4	non-motile	53.36	63.66	60.18	IlvH	Pfl01_4787 ←	5402642	Missense	G150S	GGC→AGC
5.10a	M5	motile	56.96	56.62	55.12	IlvI	Pfl01_4788 ←	5403629	Frame shift	Frame shift	Δ23bp 1166-1188/1725 nt
5.10b	M5	motile	49.96	49.89	107.61	IlvI	Pfl01_4788 ←	5403629	Frame shift	Frame shift	Δ17bp 1172-1188/1725 nt
5.10c	M5	motile				WspR	Pfl01_1058 →	1227150	Missense	T174I	ACC→ATC
5.11a	D5	non-motile	110.47	109.78	180.81	WspE	Pfl01_1056 →	1223648	Missense	M123I	ATG→ATA
5.11b	D5	non-motile	104.23	129.78	152.89	WspE	Pfl01_1056 →	1225239	In-frame Δ	Δ653-656	Δ12bp 1960-1971/2295 nt
5.11c	D5	non-motile	81.07	77.14	96.70	WspE	Pfl01_1056 →	1224144	Missense	D289N	GAC→AAC
5.11d	D5	non-motile	128.07	115.76	132.55	DgcH	Pfl01_0050 ←	55647	In-frame Δ	Δ524-537	Δ1558-1599/2091 nt
5.11e	D5	non-motile				GcbC	Pfl01_4665 →/ → Pfl01_4666	5266677	5' UTR	+ Pfl01_2031-2032	+1316 +54/-56
5.11f	D5	non-motile				MorA	Pfl01_4876 →	5499284	Missense	E1081A	GAA→GCA
5.12	M6	motile				GcbC	Pfl01_4666 →	5266862	Missense	A44P	GCC→CCC
5.13a	D6	non-motile				MorA	Pfl01_4876 →	5499088	In-frame Δ	Δ1015-1020	Δ15bp 3046-3060/3849 nt
5.13b	D6	non-motile				GcbC	Pfl01_4666 →	5267723	Missense	A331T	GCC→ACC
6.1	D0	non-motile				WspF	Pfl01_1057 →	1226544	Frame shift	KI325R*	Δ974/1011 nt
6.2a	M1	motile				WspA	Pfl01_1052 →	1219239	Duplication	L23 2→3	+3bp 69/1623
6.2b	M1	motile				WspR	Pfl01_1058 →	1227374	Missense	G249C	GGC→TGC
6.3	D1	non-motile				WspA	Pfl01_1052 →	1219239	Duplication	L24 3→2	-3bp 69/1623
6.4	M2	motile	51.19	81.77	61.87	WspE	Pfl01_1056 →	1225435	Frame shift	748*	+1bp 2156/2295 nt
6.5a	D2	non-motile	189.04	141.94	135.43	DgcY	[Pfl01_3505]–Pfl01_3506	3985701	In-frame Δ	124* Δ5' UTR 3508	Δ3505,Δ3506,Δ3508 5'UTR
6.5b	D2	non-motile				SadC	Pfl01_4451 ←	5013023	5' UTR	5' UTR	A→C (-11)
6.6a	M3	motile	69.41	59.49	94.44	DgcY	[Pfl01_3500]–Pfl01_3510	3981080	In-frame Δ	Δ10 proteins	Δ3500-3510
6.6b	M3	motile				SadC	Pfl01_4451 ←	5012937	In-frame Δ	25L 4→3	Δ74-76/1107 nt
6.7a	D3	non-motile				CheB	Pfl01_1567	1758645	Frame shift	Frame shift	Δ1bp 1061/1137 nt
6.7b	D3	non-motile				FlgF	Pfl01_1501 →	1680303	Frame shift	Frame shift	Δ14bp 138-151/741 nt
6.7c	D3	non-motile	66.67	50.69	60.25	YfiN	Pfl01_0692 →	818803	Missense	G157C	GGT→TGT
6.7d	D3	non-motile				DgcH	Pfl01_0050 ←	55952	Frame shift	Δ430	Δ1292-1294/2091 nt
6.7e	D3	non-motile				YfiR	Pfl01_0691 →	817876	In-frame Δ	Δ37-61	Δ114-188/576 nt
6.8a	M4	motile	41.34	42.22	39.91	CdrB	Pfl01_0652 ←	763630	Missense	A290T	GCC→ACC
6.8b	M4	motile				YfiN	Pfl01_0692 →	819458	Missense	A375V	GCG→GTG
6.8c	M4	motile				YfiN	Pfl01_0692 →	818709	Frame shift	Frame shift	+1bp 375/1269 nt
6.9a	D4	non-motile				DgcH	Pfl01_0050 ←	55978	Missense	L423P	CTC→CCC
6.9b	D4	non-motile				MorA	Pfl01_4876 →	5499015	Missense	M991I	ATG→ATA
6.9c	D4	non-motile				MorA	Pfl01_4876 →	5499015	Missense	M991I	ATG→ATT
6.9d	D4	non-motile				DgcH	Pfl01_0050 ←	55647	In-frame Δ	Δ524-537	Δ1558-1599/2091 nt
6.9e	D4	non-motile				GcbC	Pfl01_4665 →/ → Pfl01_4666	5266677	5' UTR	+ Pfl01_2031-2032	+1316 +54/-56
6.9f	D4	non-motile				RapA	Pfl01_1678 ←	1873535	Missense	S317A	TCG→GCG
7.1	D0	non-motile	187.52	146.52	156.37	WspC	Pfl01_1054 →	1222594	In-frame Δ	*wspC::D*	Δ1269-1270/1278 nt
7.2a	M1	motile				WspE	Pfl01_1056 →	1223360	Frame shift	156*	+1bp 81/2295 nt
7.2b	M1	motile				WspR	Pfl01_1058 →	1227186	Frame shift	205*	Δ1bp 557/1002 nt
7.2c	M1	motile				WspD	Pfl01_1055 →	1223058	In-frame Δ	Δ152-157	Δ459-476/684 nt
7.2d	M1	motile				WspD	Pfl01_1055 →	1223058	In-frame Δ	Δ152-157	Δ459-476/684 nt
7.3a	D1	non-motile				WspE	Pfl01_1056 →	1223648	Missense	M123I	ATG→ATA
7.3b	D1	non-motile				WspE	Pfl01_1056 →	1224162	Missense	R295C	CGC→TGC
7.4a	M2	motile				WspD	Pfl01_1055 →	1222912	Nonsense	Q105*	CAG→TAG
7.4b	M2	motile				WspE	Pfl01_1056 →	1224637	Missense	H453R	CAC→CGC
7.5	D2	non-motile				SadC	Pfl01_4451 ←	5013023	5' UTR	5' UTR	A→C (-11)
7.6	M3	motile				SadC	Pfl01_4451 ←	5012937	In-frame Δ	25L 4→3	Δ74-76/1107 nt
7.7	D3	non-motile				MorA	Pfl01_4876 →	5498240	Missense	S733L	TCG→TTG
8.1	D0	non-motile				WspF	Pfl01_1057 →	1226036	Missense	I156R	ATC→CGA
8.2a	M1	motile				WspC	Pfl01_1054 →	1222439	Nonsense	Q372*	CAG→TAG
8.2b	M1	motile				WspD	Pfl01_1055 →	1223283	Missense	*228C (WspD::E)	TGA→TGC
8.3a	D1	non-motile				GcbC	Pfl01_4665 →/ → Pfl01_4666	5266677	5' UTR	+ Pfl01_2031-2032	+1316 +54/-56
8.3b	D1	non-motile				MorA	Pfl01_4876 →	5499015	Missense	M991I	ATG→ATA
8.3c	D1	non-motile				MorA	Pfl01_4876 →	5499286	Missense	E1082K	GAA→AAA
8.4	M2	motile				MorA	Pfl01_4876 →	5497033	Frame shift	487*	+4bp 991/3849nt
8.5a	D2	non-motile				DgcH	Pfl01_0050 ←	55773	In-frame Δ	Δ413-491	Δ1237-1473/2091 nt
8.5b	D2	non-motile				DgcX	Pfl01_3550 →	4023270	Missense	M350I	ATG→ATA
8.6	M3	motile				DgcX	Pfl01_3550 →	4023085	In-frame Δ	Δ289	Δ3bp 865-867/1680 nt
8.7a	D3	non-motile				YfiN	Pfl01_0692 →	818891	Missense	P186R	CCG→CGG
8.7b	D3	non-motile				FliI	Pfl01_1539 →	1729003	Frame shift	Frame shift	+1bp 1015/1359 nt
9.1	D0	non-motile				WspF	Pfl01_1057 →	1226393	Missense	G275W	GGG→TGG
9.2	M1	motile				WspE	Pfl01_1056 →	1223361	Frame shift	38*	Δ82-127/2295 nt
9.3	D1	non-motile				YfiN	Pfl01_0692 →	818803	Missense	G157S	GGT→AGT
9.4	M2	motile				YfiN	Pfl01_0692 →	819523	Nonsense	Q397*	CAA→TAA
9.5a	D2	non-motile				DgcH	Pfl01_0050 ←	55896	In-frame Δ	Δ445-450	Δ1333-1350/2091 nt
9.5b	D2	non-motile				DgcH	Pfl01_0050 ←	55647	In-frame Δ	Δ524-537	Δ1558-1599/2091 nt
9.6a	M3	motile				tRNA	Pfl01_R0084 ←	5451395	5' UTR	5' UTR	G→T 49/77nt
9.6b	M3	motile				RplV	Pfl01_5074 ←	5702436	Missense	A43T	GCC→ACC
10.1	D0	non-motile	301.71	271.29	205.50	DgcH	Pfl01_0050 ←	55835	In-frame Δ	Δ467-470	Δ1400-1411/2091 nt
10.2	M1	motile	48.63	48.06	46.64	CalM	Pfl01_1895 →	2166348	Frame shift	Frame shift	+5bp 1685/2652 nt

10.3a	D1	non-motile				CalM	Pfl01_1895 →	2166348	In-frame Δ	In-frame Δ	-5bp 1685/2652 nt
10.3b	D1	non-motile				WspF	Pfl01_1057 →	1226204	Nonsense	E212*	GAA→TAA
10.3c	D1	non-motile				CalM	Pfl01_1895 →	2166348	In-frame Δ	In-frame Δ	-5bp 1685/2652 nt
10.4	M2	motile				WspR	Pfl01_1058 →	1226823	Missense	L65Q	CTG→CAG
10.5	D2	non-motile				CalM	Pfl01_1895 →	2166348	In-frame Δ	In-frame Δ	-5bp 1685/2652 nt
11.1	D0	non-motile	80.66	94.75	112.01	WspA	Pfl01_1052 →	1220312	Missense	A381V	GCC→GTC
11.2	M1	motile	49.17	51.38	65.08	RndA	Pfl01_2749 ←	3170622	Nonsense	Q51*	CAG→TAG
11.3	D1	non-motile	147.33	132.67	152.43	DgcH	Pfl01_0050 ←	55647	In-frame Δ	Δ524-537	Δ1558-1599/2091 nt
11.4	M2	motile	43.58	37.94	43.96	WspR	Pfl01_1058 →	1226967	Missense	A113D	GCC→GAC
12.1	D0	non-motile				WspE	Pfl01_1056 →	1225222	Missense	D648G	GAC→GGC
12.2	M1	motile				WspC	Pfl01_1054 →	1222526	Frame shift	421*	Δ1201-1202/1278 nt
12.3	D1	non-motile				WspA	Pfl01_1052 →	1220020	In-frame Δ	Δ283-310	Δ850-933/1623 nt
13.1	D0	non-motile				WspF	Pfl01_1057 →	1225581	Missense	A4E	GCA→GAA
13.2	M1	motile				WspC	Pfl01_1054 →	1222479	Missense	H385P	CAC→CCC
14.1	D0	non-motile				WspF	Pfl01_1057 →	1226127	Missense	H186P	CAT→CCT
14.2	M1	motile				WspA	Pfl01_1052 →	1220333	Missense	S388F	TCC→TTC
15.1	D0	non-motile				WspE	Pfl01_1056 →	1225307	Duplication	673GMD 1→2	+9bp 2028/2295 nt
15.2	M1	motile				WspF	Pfl01_1057 →	1226474	Missense	S302R	AGT→CGT
16.1	D0	non-motile				WspF	Pfl01_1057 →	1225883	Missense	P105S	CCG→TCG
16.2	M1	motile				WspC	Pfl01_1054 →	1221551	Nonsense	E76*	GAA→TAA
17.1	D0	non-motile				WspF	Pfl01_1057 →	1226391	Missense	T274I	ACA→ATA
17.2	M1	motile				WspA	Pfl01_1052 →	1219453	Nonsense	Q95*	CAG→TAG
18.1	D0	non-motile				WspF	Pfl01_1057 →	1225721	In-frame Δ	Δ48-52	Δ151-165/1011 nt
18.2	M1	motile				WspR	Pfl01_1058 →	1226688	Nonsense	L20*	TTG→TAG
19.1	D0	non-motile				WspA	Pfl01_1052 →	1220020	In-frame Δ	Δ283-310	Δ850-933/1623 nt
19.2	M1	motile				WspE	Pfl01_1056 →	1223907	Frame shift	Frame shift	-1 bp 628/2295
20	D0	non-motile				WspF	Pfl01_1057 →	1226559	Nonsense	L330*	TTG→TAG
21	D0	non-motile				WspF	Pfl01_1057 →	1225721	In-frame Δ	Δ48-52	Δ151-165/1011 nt
22	D0	non-motile				WspA	Pfl01_1052 →	1220020	In-frame Δ	Δ283-310	Δ850-933/1623 nt
23	D0	non-motile				WspF	Pfl01_1057 →	1225883	Missense	P105S	CCG→TCG
24	D0	non-motile				MorA	Pfl01_4876 →	5499286	Missense	E1082K	GAA→AAA
25	D0	non-motile				WspE	Pfl01_1056 →	1224324	Missense	R349S	CGC→AGC
26	D0	non-motile				MorA	Pfl01_4876 →	5498817	Missense	M925I	ATG→ATA
27.0 **	M0	motile				WspC	Pfl01_1054 →	1221330	In-frame Δ	Δ*wspCD*	Δ1954/1954 nt
27.1	D0	non-motile				DgcH	Pfl01_0050 ←	55873	Missense	Q458P	CAG→CCG
27.2	M1	motile	42.70	39.96	36.29	DgcH	Pfl01_0050 ←	56803	Missense	Q148P	CAG→CCG
27.3a	D1	non-motile	47.26	71.96	72.99	IlvH	Pfl01_4787 ←	5402983	Missense	A36E	GCG→GAG
27.3b	D1	non-motile				FlgL	Pfl01_1507 ←	1687852	Frame shift	326*	Δ1bp 866/1572 nt
27.4	M2	motile				WspB	Pfl01_1053 →	1221329	Missense	*179C (WspB+)	TGA→TGC
27.5	D2	non-motile				MorA	Pfl01_4876 →	5498222	Missense	V727A	GTA→GCA
ΔrsmE *	M0	motile	61.11	61.63	60.13	RsmE	Pfl01_1912 ←	2185977	In-frame Δ	Δ*rsmE*	Δ1-195/195 nt
28.1	D0	non-motile				WspA	Pfl01_1052 →	1220020	In-frame Δ	Δ283-310	Δ850-933/1623 nt
28.2	M1	motile				WspA	Pfl01_1052 →	1220716	Nonsense	Q516*	CAG→TAG
29.1	D0	non-motile				WspE	Pfl01_1056 →	1225506	Missense	K743Q	AAG→CAG
29.2a	M1	motile				WspC	Pfl01_1054 →	1221416	Frame shift	51*	+ 19bp 91/1278 nt
29.2b	M1	motile				WspA	Pfl01_1052 →	1219453	Nonsense	Q95*	CAG→TAG
30.1	D0	non-motile				WspF	Pfl01_1057 →	1226123	Nonsense	Q185*	CAG→TAG
30.2a	M1	motile				WspR	Pfl01_1058 →	1227012	Frame shift	138*	Δ1bp 383/1002 nt
30.2b	M1	motile				WspC	Pfl01_1054 →	1222448	Frame shift	389*	Δ1bp 1123/1278 nt
31.1	D0	non-motile				WspC	Pfl01_1054 →	1222342	In-frame Δ	WspC::D	Δ305bp WspC:WspD
31.2a	M1	motile				WspA	Pfl01_1052 →	1220714	Missense	R515P	CGT→CCT
31.2b	M1	motile				WspA	Pfl01_1052 →	1220099	Missense	T310N	ACC→AAC
32.1	D0	non-motile				WspE	Pfl01_1056 →	1225223	Missense	D648G	GAC→GAA
32.2a	M1	motile				WspA	Pfl01_1052 →	1219957	Missense	S263P	TCC→CCC
32.2b	M1	motile				WspB	Pfl01_1053 →	1221235	Nonsense	W148*	TGG→TAG
33.1	D0	non-motile	86.13	60.82	85.85	WspF	Pfl01_1057 →	1225721	In-frame Δ	Δ48-52	Δ151-165/1011 nt

§ Relationships of the lineages presented here are visualized in Fig. S1. Strain IDs correspond to variant calling files found in 'Table S1 - Source Data 1' that provides evidence for each reported mutation. All strains were generated in this experiment unless otherwise noted or stated here: * (Kim et al., 2014); ** (Kim et al., 2016); # (Compeau et al., 1988). M and D served as the prototype ancestral strains throughout this study.

§§ Generation refers to an individual strain's evolutionary distance from WT where the following sequence represents the accumulation of mutations at each generation: WT, M0, D0, M1, D1, … M6, D6.

† Determined by stab-motility assays.

‡ Select strains were chosen for LC-MS/MS c-di-GMP quantification conducted in triplicate.

*** Locus, CDS, and Mutation Location (NT) were extracted from GenBank reference CP000094 unless otherwise stated. CDS: → (+ strand), ← (- strand), / (intergenic space). Genotype (AA/NT) was reported by BreSeq during variant analysis. Consequence describes the nature of mutation.

Table S2. Node-edge plot data matrix*.

Source	Target	Attribute	Count
CdrB	DgcH	D	1
CdrB	MorA	D	1
ParA	WspA	D	1
ParA	WspB	D	1
CalM	CalM	D	2
CalM	WspF	D	1
RndA	DgcH	D	1
NarA	WspD	M	1
DgcY	Pfl01_1567	D	1
DgcY	FlgF	D	1
DgcY	DgcY	M	1
DgcX	Pfl01_1539	D	1
DgcX	YfiN	D	1
DgcX	DgcX	M	1
SadC	DgcH	D	2
SadC	IlvH	D	1
SadC	MorA	D	1
SadC	WspE	D	2
SadC	YfiN	D	2
SadC	YfiR	D	1
SadC	SadC	M	4
DgcH	FlgL	D	1
DgcH	IlvH	D	1
DgcH	WspA	D	2
DgcH	WspF	D	1
DgcH	CalM	M	1
DgcH	DgcH	M	2
DgcH	R0084	M	1
DgcH	RplV	M	1
DgcH	WspR	M	1
GcbC	DgcY	D	1
GcbC	GcbC	D	1
GcbC	MorA	D	2
GcbC	GcbC	M	1
IlvH	ParA	M	1
IlvH	WspB	M	1
IlvI	DgcH	D	1
IlvI	WspE	D	3
MorA	DgcX	D	1
MorA	DgcH	D	1
MorA	MorA	M	1
RsmE	DgcH	D	2
RsmE	WspA	D	4
RsmE	WspD	D	1
RsmE	WspE	D	2
RsmE	WspF	D	15
RsmE	WspD	M	1
WspA	NarA	D	1
WspA	DgcH	D	1
WspA	WspA	D	3
WspA	WspE	D	2
WspA	RndA	M	1
WspA	WspA	M	4
WspA	WspB	M	1
WspA	WspD	M	3
WspA	WspE	M	5
WspB	MorA	D	1
WspB	WspE	D	2
WspB	IlvI	M	2
WspC	DgcH	D	1
WspC	WspA	D	2
WspC	WspE	D	1
WspC	WspD	M	2
WspC	WspE	M	1
WspC	WspR	M	1
WspD	Pfl01_1562	D	1
WspD	Pfl01_1757	D	1
WspD	SadC	D	3
WspD	GcbC	D	2
WspD	MorA	D	2
WspD	WspA	D	1
WspD	WspD	D	1
WspD	WspE	D	3
WspD	WspA	M	3
WspE	Pfl01_3026	D	1
WspE	DgcY	D	1
WspE	SadC	D	2
WspE	DgcH	D	2
WspE	GcbC	D	1
WspE	MorA	D	2
WspE	WspA	D	2
WspE	WspE	D	1
WspE	YfiN	D	1
WspE	WspA	M	2
WspE	WspB	M	1
WspE	WspC	M	2
WspE	WspE	M	2
WspE	WspR	M	2
WspF	WspA	M	4
WspF	WspC	M	4
WspF	WspD	M	1
WspF	WspE	M	2
WspF	WspR	M	4
WspR	CalM	D	2
WspR	GcbC	D	1
WspR	MorA	D	1
WspR	YfiN	D	1
YfiN	DgcX	D	1
YfiN	DgcH	D	3
YfiN	GcbC	D	2
YfiN	IlvH	D	1
YfiN	MorA	D	3
YfiN	RapA	D	1
YfiN	WspE	D	2
YfiN	CdrB	M	1
YfiN	YfiN	M	4
YfiR	YfiN	M	1

* Values are reported in to-from format with source indicating the mutation a parent strain carries, target indicating the mutation a daughter cell carries, attribute indicating if said daughter cell's mutation resulted in the M or D phenotype, and count indicating the frequency of the pattern in the dataset.

Table S3. Description of PCR primers used to reconstruct mutations.

Target mutation	Forward Primer Sequence	Reverse Primer Sequence
WspA::D	ATCTGGTGAACGCCAAACT	TGACCAGGCAATCTTCCATC
WspB::D	CCACGTATGACATCGAACAGA	CTGTCGAGATCGAGCAGTTC
WspC::D	TGCCGAGAACGAAGGTTA	CTGTCGAGATCGAGCAGTTC
IlvH (A36E)	CAAGACGGAGCGTACCTAATC	AACGGTAGCCGAACCTTTAC
IlvH (S149R)	CAAGACGGAGCGTACCTAATC	AACGGTAGCCGAACCTTTAC
IlvH (G150S)	CAAGACGGAGCGTACCTAATC	AACGGTAGCCGAACCTTTAC
IlvI (Δ17bp)	AGGGAAGCTCAAAGCGATAC	AACCTGCCGGTTACCAATAC
IlvI (Δ 23bp)	AGGGAAGCTCAAAGCGATAC	AACCTGCCGGTTACCAATAC
DgcY (Δ3505-3506)	ATGGCTAAGCCCAGTTACACA	TGAAGCCGTTGAGATCGATA
DgcY (Δ3500-3510)	ATCGTTAGGGCGCTATCAATAC	TTGCATCGAGCAGGGTTTTC
NarA (A383S)	CATTTACACCTCGGGAGATGAC	CGACAGCGCATTGAAGAAAC
CalM (+5bp)	CTGCTGACCAATCCAATCCT	AAGTCATCGTCTGCCAACTC
RndA (Q51S)	TTGTTCACTCATCGCCTACTG	CGACCAGCGTTCCGATAAA
CdrB (A290T)	CGTTATCAACAGGACGGCTATC	GCTTGAGTTCCAGACCGTTATT
ilvH external check	CGCACTCCTACATGGAATCA	CAGCTACATCGGTCACTTTCA
ilvI external check	AAGCCAAACTGCGTTCCTA	TTCATCTGGATACTGCCTTCAC